Edited by

Dale A. Quattrochi

Michael F. Goodchild

Scale in Remote Sensing and GIS

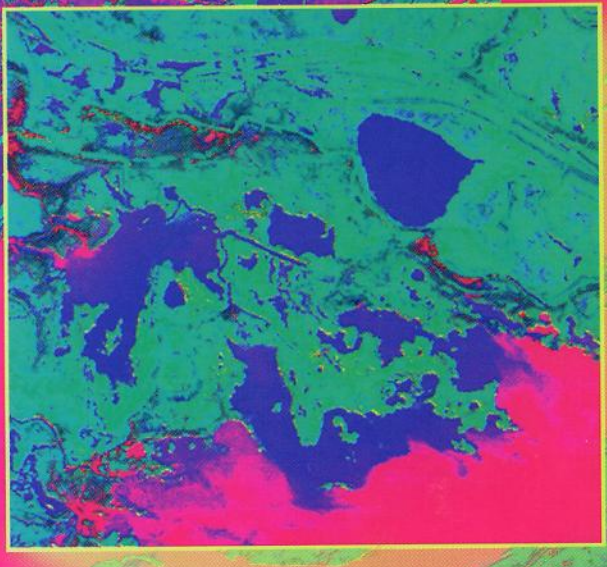

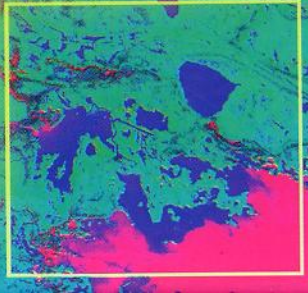

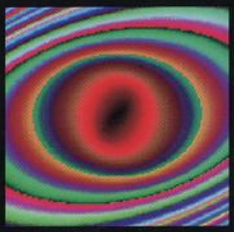

Scale in Remote Sensing and GIS

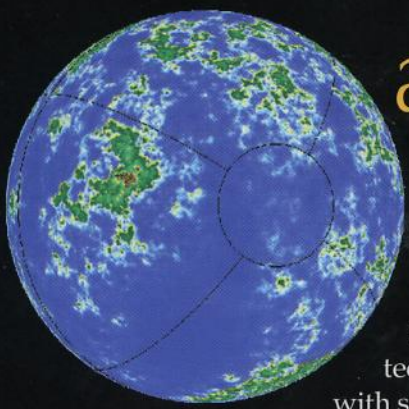

The recent emergence and widespread use of remote sensing and geographic information systems (GIS) has prompted new interest in scale as a key component of these and other geographic information technologies. Techniques for dealing explicitly with scale are now available in GIS, but, until now, very little literature was available to consider and solve specific issues of scale.

With a balanced mixture of concepts, practical examples, techniques, and theory, ***Scale in Remote Sensing and GIS*** is a guide for students and users of remote sensing and GIS who must deal with the issues raised by multiple temporal and spatial scales.

The book explores issues of scale in three broad areas:

- Spatial/temporal statistical analysis and model development
- Multiple scaled data for analysis of the biophysical environment
- Multiple scaled data for model development and analysis in landscape ecology

Written by a team of specialists in remote sensing data and GIS, this book offers readers new ways to relate, manipulate, and otherwise use and understand spatial data. Profusely illustrated, ***Scale in Remote Sensing and GIS*** contains over 24 full-color photographs to help demonstrate key points made in the text.

L1104

ISBN 1-56670-104-X

90000

9 781566 701044

CHAPTER 16

Multifractals and Resolution Dependence of Remotely Sensed Data: GSI to GIS

Sean Pecknold, Shaun Lovejoy, Daniel Schertzer, and Charles Hooge

INTRODUCTION

The Zonal Aggregation Problem: From Fractal Sets to Multifractal Measures

Geographers have long sought to provide complete representations of spatial information. For example, maps are based on the notion of "cartographic scale," which is in fact a scale ratio — but not a spatial resolution. Implicitly, the attempt is made to represent everything of "geographical significance" (irrespective of actual size); the aim is provide a one to one correspondence with reality. When the information can be reduced to geometric sets of points, various techniques for conceptualizing it have been developed. For example, topology and distance information can be dealt with using notions of "nodes," "links," "networks," hierarchies," "spheres of influence" (e.g., O'Brien 1992). However, when the number of relevant points is extremely large (such as the location of each individual human being, completely representing the population distribution, or the location and size of each tree needed to completely specify the "forest cover") this complete representation is often unwieldy, if not technically impossible to achieve. Hence the need for "zonal aggregation," i.e., spatial integration or averaging. Attempts to do this have led to the recognition of the "ecological fallacy"; the fact that the level of aggregation is fundamentally important in determining the statistical properties of the set of interest. Similar scale problems appear in the context of image-mapping and generalizations, and for data abstraction and database building for multiscale representations.

1-56670-104-X/97/$0.00+$.50
© 1997 by CRC Press, Inc.

In the last ten years, encouraged by the explosion of scaling and fractal ideas in geophysics and elsewhere, there have been attempts to overcome the aggregation problem by recognizing that many spatial processes have no characteristic size: hence, that the corresponding sets are fractals. This means that over wide ranges (in at least certain cases such as the atmosphere, spanning nine or ten orders of magnitude in scale) there is no homogeneity scale (i.e., below which the variability is small enough to ignore), and the resolution is therefore fundamental. In remotely sensed data — increasingly used for quantitative studies — the resolution ("pixel" size) is always explicit, but is often much larger than this "optimum" resolution,[1] which for geophysical systems can readily be of the order of millimeters or less. Over a certain range (the scaling range), these geometric fractal sets exhibit scaling, i.e., having densities, lengths, areas, or other measures of size which are power law functions of the spatial resolution. The basic quantity of interest is the exponent which determines the rate of change of these measures with resolution — the scaling exponent. The examples of the coastline set of Britanny (Perrin, 1913), and Britain (Richardson, 1961; Mandelbrot, 1967), whose tangent (Perrin, 1913) and length (Richardson, 1961; Mandelbrot, 1967) change systematically with resolution are now well-known. For such geometric sets, the standard aggregation problem is simply ill-posed; the result — the length of the coast of Britain — is just a strong (scaling) function of the subjective observer/map resolution, it is not an objective characteristic of the coastline. It is now generally recognized that the coastline length has no geographical significance per se.

While the growing recognition that scaling is a basic feature of geographic sets is an important advance, it has contributed to the unfortunate tendency to reduce geographical features and information to geometric sets (whether scaling or otherwise). The inadequacy of the set framework is perhaps becoming most obvious in recent attempts to integrate both traditional "vector" data (i.e., the coordinates of geometric points) with increasing quantities of remotely sensed "raster" (i.e., pixel-based) data into geographic information systems (GIS; Davis and Simonett, 1991, have called the result an Integrated GIS = "IGIS"). Since remotely sensed data usually have significant intensity information at each pixel, the satellite brightness is more appropriately represented as a mathematical field rather than as a geometric set of points (actually, the satellite integrates radiances over pixels — it is sufficient and indeed preferable to theorize the latter as a mathematical measure). Indeed, it turns out that the more general measure/field framework is often preferable even for treating geometric sets — it is the (multifractal) density of the latter which is of interest! For example Tessier et al. (1994) have shown that it is much more convenient to treat the meteorological measuring network as density fields representing the number of stations/area. Similarly, we anticipate (Tessier et al., 1995) that it is better to treat forest cover as a field representing the density of trees, rather than as a set of points.

The same scale invariant symmetry considerations that lead us to treat scaling sets as fractals also hold for scale invariant fields; however the latter are generally "multifractals." That is, rather than having lengths, or other measures of size varying

[1] The notion of "optimum resolution" can be defined in many ways; here we take it as equal to the scale below which the phenomenon is homogeneous.

according to power laws (characterized by a unique exponent, the fractal dimension), multifractals have an infinite hierarchy of exponents (an exponent function). In practice their characterization involves a reliance on various universality properties (see below) that allow the infinite hierarchy to be reduced to a finite (and manageable) number. While the discovery and investigation of the properties of multifractals and multifractal processes are undoubtedly the most significant single advance in scaling notions in the last fifteen years, it is surprising that so far their significance for geography has been little appreciated (see however, De Cola and Lam, 1993; Lavallée et al., 1993b). Indeed, although it took nearly 70 years for the inappropriateness of the (fractal) question "how long is the coast of Brittany?" to become obvious for all, it is surprising that the corresponding multifractal question "how bright is the coast of Brittany?" is still being answered in terms of fractional cloud cover or using other resolution dependent notions (see Lovejoy and Schertzer, 1995, for a discussion and review).

Generalized Scale Invariance (GSI), Universality and Self-Organized Criticality

Geographers are not alone in underestimating the significance of scale invariance and multifractals. Some of us have argued (Schertzer and Lovejoy, 1996) that even in physics, where multifractals are well-established, their scope has been underestimated for a series of reasons. The first such reason, discussed below, is that although a general framework for anisotropic scale invariance has existed for over ten years (generalized scale invariance — GSI — Schertzer and Lovejoy, 1983, 1985b, 1987, 1989, 1991b), in most of the literature scale invariance has been restricted to isotropic (self-similar) systems and few (if any) natural systems are isotropic. Occasionally extensions have been made to accommodate anisotropy along coordinate axes ("self-affinity"; the privileged directions are fixed in orientation), but this is still quite restrictive.[2] The formulation of scale invariance as a symmetry principle (GSI) also provides an explanation for the widespread scaling found in natural systems: Table 1 shows over 20 geophysical fields in which multiscaling has been established, indicating the range of scales over which this multiscaling behavior is observed along with the universal multifractal parameters determined from them (explained in detail below), giving the "multifractality" of the field: α, its sparseness: C_1, and its "smoothness": H. Just as with other more familiar symmetries, such as conservation of momentum or energy, we may expect scaling symmetries to be respected unless strong scale breaking mechanisms exist. With the development of GSI, the ubiquity of scaling is no more of a mystery than is the conservation of energy.

The second aspect of multifractals which has been under-appreciated is the fact that, unlike fractal geometry which simplifies things by introducing a single exponent, in multifractals, the exponent is a function; this is equivalent to an infinite number of exponents (see below for a discussion). In other words, with no other information, multifractals would be unmanageable both theoretically and empiri-

[2] It has also been badly misused as a monofractal model for a multifractal field. Perhaps the most obvious example is the attempt to reduce a multifractal field such as topography to a self-affine, and hence monofractal, geometric set. See Lavallée et al. (1993a) for a discussion.

cally. Fortunately, multifractal processes possess stable, attractive generators and thus can have universal behavior governed by only three fundamental parameters[3] (Schertzer and Lovejoy, 1987, 1996; Schertzer et al., 1991), as given in Table 1. This can be regarded as a generalization (and mathematical and physical development) of the old idea of the law of "proportional effect" (Kapteyn, 1903; originally believed to lead to log-normal distributions). Finally, unlike the special (geometric, microcanonical) multifractals usually treated in the literature, the more general canonical multifractals are extremely variable, giving rise to extreme fluctuations, characterized by qualitative changes called "multifractal phase transitions."Recently, it has been shown (Schertzer and Lovejoy, 1994) that certain generic first order transitions are in fact a nonclassical form of self-organized criticality (Bak et al., 1987). Multifractals can therefore naturally account for the extreme events which characterize so many geophysical and geographical systems.

The arguments we have presented about the relevance of multifractals to geography and to remote sensing are not entirely new; relevant discussions can be found in Lavallée et al. (1993b), Lovejoy and Schertzer (1995) and Schertzer and Lovejoy (1995b). The aim of the present paper is rather to illustrate multifractal analysis and modeling techniques on four fields of geophysical and geographical significance: the cloud radiance field, the sea ice radar reflectivity field, the aeromagnetic field, and the topography field. In each case, we combine estimates of the universal multifractal parameters with those of the anisotropy (GSI) in order to make realistic simulated realizations. Readers who remain skeptical about the theoretical justification for multifractals are invited to scan the latter and judge by the visual and statistical realism that the simulation technique provides.

SCALING, MULTIFRACTALS AND UNIVERSALITY

The word "fractal" was coined by Mandelbrot (Mandelbrot, 1975) to describe the fractured and fragmented appearance of fractal sets; an early example was that of coastlines and other aspects of topography. Even before that, the question of the length of a coastline (Richardson, 1961; Mandelbrot, 1967) was recognized as an aspect of a paradox noted even earlier (Steinhaus, 1954): that the size/measure of an object depended on the scale at which it was examined (the example being that of the measurement of the left bank of the river Vistula: when measured with increased precision, the length would be much larger than the length read off a less precise map). This yields the twin notions of scaling — the (power-law) dependence of a measured quantity on the scale at which it is measured — and the fractal geometric set, with a non-integer dimension; the statistical properties of a fractal set (such as aggregation complexity) are determined by a single fractal dimension. In fact, this is a scaling relationship: the "size" of a fractal set varies as the scale at which it is examined raised to a (scale invariant) scaling exponent, in this case given by the fractal dimension.

[3] Note however the debate about strong vs. weak universality below.

Later, with the development of the more general scaling framework needed to handle scale invariant fields, there came a transition to the concept of multifractal fields and measures (Grassberger, 1983; Hentschel and Procaccia, 1983; Schertzer and Lovejoy, 1983, 1985b, 1987; Lovejoy and Schertzer, 1985; Parisi and Frisch, 1985; Meneveau and Sreenivasan, 1987). Multifractal fields are those characterized by multiscaling behavior: the scaling properties of the field are characterized by a scaling exponent function ("Multiscaling" is therefore a precise mathematical notion.) Rather than being described by a single fractal dimension, in fact a multifractal field can be thought of as a hierarchy of sets (corresponding for example to the regions exceeding fixed thresholds) each with its own fractal dimension (see Figure 1). Thus, if we consider the probability of finding a field value $\varepsilon_\lambda(x)$ greater than a given scale-dependent threshold, we find that the probability, $\Pr(\varepsilon_\lambda(x) > \lambda^\gamma)$, can be related to the order of singularity γ that characterizes this threshold, $\varepsilon_\lambda > \lambda^\gamma$, by:

$$\Pr\left(\varepsilon_\lambda > \lambda^\gamma\right) \approx \lambda^{-c(\gamma)} \tag{1}$$

where the codimension function, $c(\gamma)$, describes the *sparseness* of the field intensities[4] (Schertzer and Lovejoy, 1987). The significance of Eq. 1 for geography is immediately obvious, since λ is essentially a map resolution[5] (rather than the "scale" of the map, the ratio of distance on the map to distance in reality). If ε_λ represents a density of interest (such as forest cover, cloud cover, etc.) then Eq. 1 precisely determines how the histograms of the density vary with map resolution. Changing resolution can drastically change the statistical properties; only the codimension function will remain the same (see Figure 1).

An equivalent description may be made in terms of the moment scaling function, $K(q)$, which is defined as:

$$\lambda^{K(q)} \approx \langle \varepsilon_\lambda^q \rangle \tag{2}$$

This gives the scaling behavior of each moment q of the field.[6] In real systems with finite inner and outer scaling cutoffs, the multiscaling behavior (different scaling exponents for each moment) will only be observed over some finite range of scales. These however can be quite large; in the case of the atmosphere, noted above, it can

[4] When the codimension is smaller than the dimension of the space in which the process is observed, it has a geometric interpretation as the difference between the dimension of space and the fractal dimension of the geometric subset described by the singularity value.

[5] More precisely it is the square root of the ratio of the area (in 2 dimensions) of the region represented to the area of the smallest structure represented.

[6] Note that there is a growing realization (e.g., Mandelbrot, 1995) that the "codimension" formalism (given here) for multifractals is indispensable. The codimension formalism is related to the still popular dimension formalism (Halsey et al. 1986) by $f(\alpha) = D - c$, $\alpha = d - \gamma$, $\tau = (q - 1)D - K(q)$, where D is the dimension of the space in which the process is observed. In particular, the codimension formalism avoids the paradox of negative ("latent") fractal dimensions, has the advantage that it gives an intrinsic characterization of the process, independent of D, and can be applied to infinite dimensional probability spaces ($0 \rightarrow \infty$).

Table 1 Multifractal Parameters and Multiscaling Ranges Determined for a Variety of Geophysical Fields

Field	Type	α	C_1	H	Range of scales
Radiation fields	Clouds, Visible, Infra red[a]	1.35	0.15	0.3–0.4[b]	160 m → 4000 km
	Clouds Microwave[b1]	1.35	0.10	0.3–0.5[b]	10 km → 2000 km
	Ocean color[hh]	2.0	0.05	0.15	7 m → 200 km
Rain	Rain Radar reflectivity[c]	1.35	0.30	0.0	30 m → 64 km
	Raingauge, horizontal[c]	1.35	0.20	0.0	50 km → 4000 km
	Raingauge, time series[f]	0.5–0.7	.45–.60	0.0–0.1	8 minutes → 16 days[h]
Rivers	Daily streamflow[i]	1.45 ± .3	0.2 ± .1	−0.1 ± .1	1 month → 30 years
Turbulent velocity	Wind (tunnel, time)[j]	1.30	0.06	.33	1 ms → 1 s
	Wind atmos. (time)[k]	1.45	0.07	.33	1 ms → 1 s
	Wind atmos. (horizontal)[l]	1.35 ± .07	0.068 ± .01	0.33 ± .03	12 m → 12 km
	Wind atmos. (vertical)[m]	1.85 ± .05	.076 ± .01	0.6 ± .1[n]	50 m → 14 km
Temperatures	Climatological Temperatures	1.6[o2]	0.05[o2]	0.24[o3]	400 → 40,000 years
	Temperature (atmos., time)[p]	1.20	0.04	0.30	0.1 s → 1000 s
	Temperature, atmos. (hor.)[s]	1.25 ± .06	0.04 ± .01	.33 ± .03[s2]	12 m → 12 km
Turbulent scalars	Pollution (Seveso)[t]	1.2	0.8	−0.2	30 m → 5 km
	Oxygen concentration[gg]	1.6	0.06	.2 ± .3	10 m → 16 km
	Salinity[gg]	1.6	0.06	.1 ± .2	10 m → 16 km
	Temperature, ocean[gg]	1.6	0.06	.33	10 m → 16 km
	Plankton concentration[gg]	1.6	0.06	.0 ± .3	10 m → 16 km
	Cloud liquid water (hor.)[u]	2.00 ± .01	0.07 ± .01[v]	0.28 ± .03[v]	5 m → 330 km
Measuring networks	Density of stations[w]	0.8	0.3	0.0	200 km → 20000 km
Surfaces	Sea Ice (radar)[x]	1.85 ± .05	0.01 ± .01	−.15 ± .05	50 m → 25 km
	Ocean surface (0.95 μm)[y]	1.1	0.25	0.35	1 m → 50 m
	Topography[aa]	1.8 ± .1	0.06 ± .01	0.5 ± .02	50 m → 10,000 km
	Rock fracture surfaces[ab]	1.5	0.30	0.80	50 μm → 5 cm
Astrophysics	Galactic luminoscity[bb]	1.2 ± 0.4	1.3 ± 0.1	0.0	0.1 → 100°
Solid Earth	Seismicity[cc]	1.1	1.35	0.0	2 km → 1000 km
	Geomagnetic field[ee]	1.9	0.09	0.7	400 m → 100 km
Physiology	Low frequency speech[ff]	2.0	0.1	−0.35	0.1 s → 1000 s

[a] (Tessier et al., 1993b; see also Lovejoy and Schertzer, 1993).
[b] The value of H depends slightly on the wavelength band used.
[b1] At 19, 21, 37 GHz (Lavallée et al., 1993a), the value of H depends slightly on the wavelength band used.
[c] (Tessier et al., 1993b).
[f] Tessier et al. (1993b) and Ladoy et al. (1993) obtain similar values for the global network and Nimes respectively (for 12 hour, 24 hour resolution, respectively). Other similar values were obtained in Réunion and Dédougou (Hubert et al., 1993). Nguyen et al. (1993) find a slighly larger α, smaller C_1 in various locations near Montreal.
[h] Using a very large data base, Olsson et al. (1995) find similar values in Lund, Sweden, over periods of 8 minutes to 1 week.
[i] (Tessier et al., 1996c), 50 rivers.
[j] (Schmitt et al., 1992a), note that the theoretical (Kolmogorov) value of H is 1/3.
[k] (Schmitt et al., 1994).
[l] (Chigirinskaya et al., 1994).
[m] (Lazarev et al., 1994), radiosondes.
[n] H was first estimated using Jimspheres, by Endlich and Mancuso (1968), and confirmed by Adelfang (1971), and Schertzer and Lovejoy (1985a). The theoretical (Bogliano-Obhukov) value of H is 3/5.
[o2] (Schmitt et al., 1995).
[o3] (Lovejoy and Schertzer, 1986), analysis of hemispheric temperatures and ice core paleotemperatures.
[p] (Schmitt et al., 1992b), the theoretical value for H is 1/3 if it is approximated as a passive scalar.
[s] (Chigirinskaya et al., 1994).
[s2] The theoretical value (passive scalar approximation) is 1/3.
[t] (Salvadori et al., 1993).
[u] (Brosamlen, 1993). The value $\alpha \approx 2$ may be an artifact of the measuring device which poorly estimates the low density region.
[v] Davis et al. (1994) obtained similar values for H, C_1 with a smaller data set. The theoretical value (passive scalar approximation) is 1/3.
[w] Using the global meteorological measuring network, considering the station density as a multifractal (Tessier, 1993; Tessier et al., 1994a).
[x] Synthetic aperture radar, 10, 30 cm wavelengths, all polarizations (Falco et al., 1995).
[y] (Tessier et al., 1993c).
[aa] Deadman's Butte, Wyoming, 50 to 25 km, France, 1 to 1000 km (Lavallée et al., 1993b), present paper, etopo 5: 10 km to planetary scale, unpublished analysis.
[ab] (Schmittbuhl et al., 1995).
[bb] (Garrido, et al.).
[cc] (Hooge, 1993; Hooge et al., 1994).
[ee] (Hooge et al., 1995).
[ff] (Larnder et al., 1992).
[gg] (Tessier et al., 1996a).
[hh] Parameters are for eight visible channels, Tessier et al., 1996b.

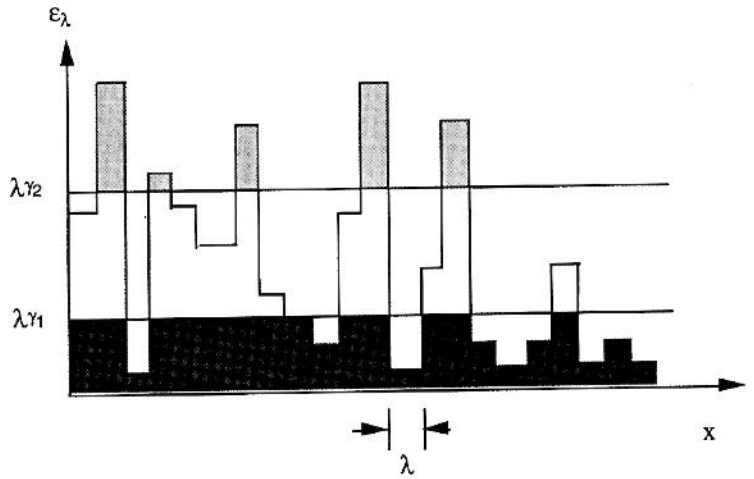

Figure 1 A schematic illustration of a multifractal field analyzed over a scale ratio λ, with two scaling thresholds λ^{γ_1} and λ^{γ_2}, corresponding to two orders of singularity: $\gamma_2 > \gamma_1$.

cover nine to ten orders of magnitude (from planetary scales to the viscous dissipation scale).

These scaling exponent functions allow a complete characterization of the statistics of the field. They are nevertheless somewhat difficult to handle, as they represent an infinite hierarchy of parameters (i.e., an arbitrary convex function). We wish to find an expression for one (or both) of these functions that will enable us to describe the scaling in a fairly simple form, with a small number of parameters. In order to do this, we note that many geophysical systems involve turbulence, which has long been regarded as arising from cascade processes (Richardson, 1922). Explicit cascade models have been developed (Novikov and Stewart, 1964; Mandelbrot, 1974; Frisch et al., 1978; Schertzer and Lovejoy, 1987), where a quantity such as energy flux (for atmospheric turbulence) is injected at large scales and cascades to smaller and smaller scales via multiplicative modulations (see Figure 2).

Under quite general conditions involving scaling non-linear cascade-like dynamics (even in the absence of strictly hydrodynamic turbulence), due to the existence of stable attractive generators of multifractal processes, cascade processes such as this are believed to result in "universal" multifractals[7] (Schertzer and Lovejoy, 1987), where the $K(q)$ function is given by

[7] Note, however, the recent debate about strong vs. weak universality (Schertzer and Lovejoy, 1995b, 1996; She and Waymire, 1995). The She-Leveque model based on a cascade of eddies postulates a recursive scaling relation between different sets of eddies, and filamentary structures for the highest order singularities. This corresponds to a weak version of universality, with an implicit assumption of an upper bound on the singularities. The strong universality discussed here has no explicit assumptions about structures in the system, and has no intrinsic maximum order of singularity.

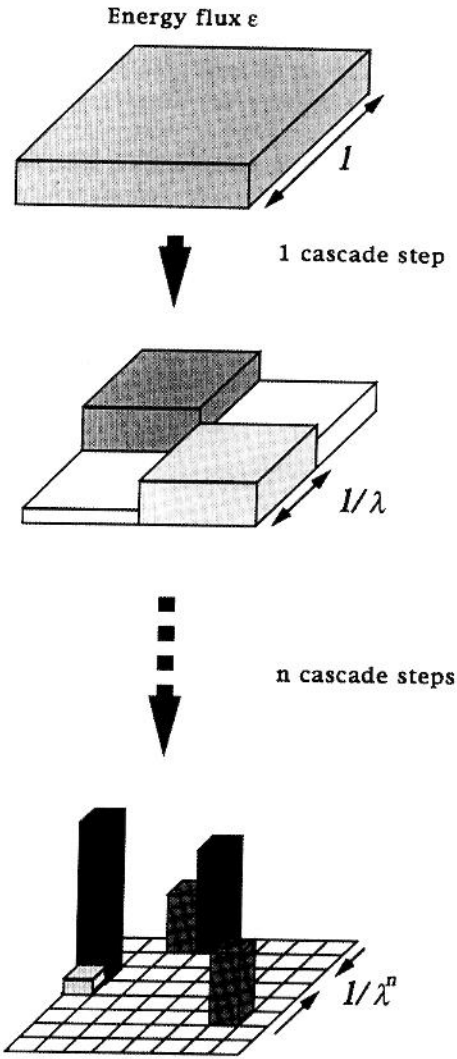

Figure 2 A schematic illustration of a multifractal field being produced by a multiplicative cascade (Schertzer and Lovejoy, 1987).

$$K(q) = \frac{C_1}{\alpha - 1}\left(q^{\alpha} - q\right), \quad \alpha \neq 1$$
$$K(q) = C_1 q \log q, \qquad \alpha = 1 \tag{3}$$

where $0 < \alpha \leq 2$. C_1 is the codimension of the mean of the field, characterizing the sparseness of the mean value of the field, and the Lévy index α characterizes the degree of multifractality (Schertzer and Lovejoy, 1987). As $\alpha \to 0$, $K(q)$ becomes linear and we obtain the monofractal β-model (Novikov and Stewart, 1964; Yaglom,

1966; Mandelbrot, 1974; Frisch et al., 1978), where the field may be described by a single dimension; the maximum value $\alpha = 2$ corresponds to the well-known lognormal model.[8] These universal multifractals have been shown to describe a large number of geophysical and other systems (see Table 1), and form the basis for the analysis and simulation techniques in this paper. Thus, our scaling exponent function is given by the two fundamental parameters α and C_1. Likewise, the codimension function $c(\gamma)$ may also be described in terms of these parameters:

$$c(\gamma) = C_1\left(\frac{\gamma}{C_1\alpha'} + \frac{1}{\alpha}\right)^{\alpha'} \tag{4}$$

with $\frac{1}{\alpha} + \frac{1}{\alpha'} = 1$.

For nonconservative fields (Schertzer and Lovejoy, 1987, 1991a) such as density fields, f_λ related to a conservative multifractal field ε_λ in a scaling manner ($|\Delta f_\lambda| = \varepsilon_\lambda \lambda^{-H}$), there is a third fundamental parameter, H, which is a measure of the degree of (scale by scale) non-conservation of the field:

$$\langle |\Delta f_\lambda| \rangle = \lambda^{-H} \tag{5}$$

If $H \neq 0$ then the universal form for $K(q)$ is given by:[9]

$$K(q) \rightarrow K(q) - qH \tag{6}$$

Examples of the effects of varying these parameters on the appearance of the system may be found in Plates 11 and 12*. In Plate 12, it is obvious that the parameter H acts as a scale invariant smoothing operator for $H > 0$, while $H < 0$ acts as a differentiation, in effect "roughening" the field more and more for decreasing H. The parameter C_1 also has a fairly obvious meaning — in Plate 11, the images on the right have a much larger C_1, resulting in most of the normalized field having a fairly small value, with a few large spikes. As α is decreased, the field (again, a normalized field) changes from one that has more symmetric deviations from the mean to one that is fairly high-valued with a few large downward deviations. This is most noticeable in the images with a lower C_1.

LINEAR GENERALIZED SCALE INVARIANCE

The second step in describing and hence modeling geophysical fields is the determination of the anisotropy present in the system. Although most systems exhibit statistical scale invariance over various ranges, *a priori* this scale invariance should

[8] This is actually a misnomer — due to divergence of moments, the distribution will only be approximately lognormal.

[9] This is true for "bare" cascade quantities. For the observed "dressed" quantities, Eq. 6 will break down below a critical value of q and trivial scaling will result (Naud et al., 1996). From the data analysis point of view, we restore the bare scaling by fractionally differentiating by order H or higher.

* Color plates follow numbered page 168.

not be expected to be isotropic (the multifractals, or fractals, will not be "self-similar"). Indeed, the only reason that isotropy is often implicitly assumed is that the anisotropic nature of most geophysical systems is usually hidden through the use of isotropic analysis techniques. For example, the Fourier power spectrum of a field is defined to include an angular integration in Fourier space that tends to "wash out" (by integrating out) all but the most severe anisotropies; nevertheless, as we show below, these do play an important part in determining the texture and morphology of the fields.

The only scaling anisotropy usually considered in the literature is "self-affine" scaling, in which anisotropy is confined to fixed coordinate axes: this is an insufficient generalization for most applications. The framework of generalized scale invariance (GSI) was developed to describe much more general scaling anisotropies. It extends the idea of scale invariance, where the small-scale and large-scale structures and behaviors are related by a scale-changing operator that depends only on the scale ratio, to include more complicated scale-dependent changes of behavior and structure, such as differential stratification and rotation. We therefore regard our systems in terms of GSI, restricting ourselves to the linear case (where the anisotropies are statistically independent of position; they depend only upon the scale ratio).

To develop the framework of GSI, we need several components. The first of these is the scale changing operator, T_λ. Scale-invariance requires that the statistical properties of a field are changed in a power-law way with an isotropic change in scale λ of space, such as zooming. T_λ is the rule relating the statistical properties at one scale to another. Since the properties only depend on the scale ratio λ and not actual sizes, T_λ must have semi-group properties; in particular it admits a generator $\mathbf{G}$ such that:

$$T_\lambda = \lambda^{-\mathbf{G}} \tag{7}$$

In the case of linear GSI, $\mathbf{G}$ is a matrix: the identity matrix for the isotropic case (see Figure 3), but a more general one for the case of self-affinity or more general anisotropies (Figure 4).

We also require a family of balls that cover the space and are acted upon by the scale changing operator (these balls define the topology of the space), as well as a way to define what we mean by scale (these requirements are described in detail in Schertzer and Lovejoy, 1985b). In many physical cases there is no overall stratification (e.g., if we study horizontal and not vertical cross-sections of the atmosphere, earth or oceans). It therefore suffices for a definition of scale to use the "obvious" one, i.e., the square root of the area of these balls. In the isotropic case the balls are in fact circles, indicating no preferred direction at any scale. In the anisotropic case, if a scale exists at which the system is isotropic, we call this scale the spheroscale. The family of balls obtained from acting upon it with T_λ will be ellipses, and the $\mathbf{G}$ matrix together with the size of the spheroscale will define our system. If no such scale exists, it may be necessary to define a somewhat more complicated family of balls; one such family is of fourth-order closed polynomial balls (Pecknold et al., 1996) (see Figure 5).

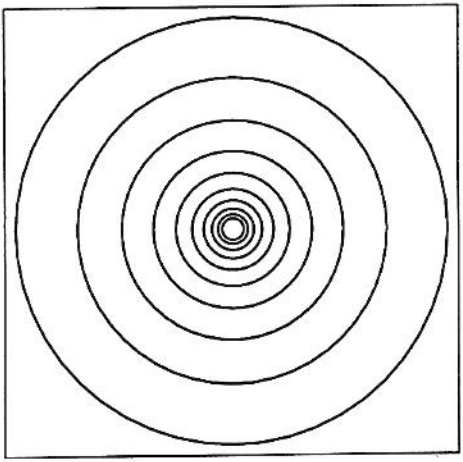

Figure 3 A schematic illustration of the shape of the mean structures as functions of scale in self-similar scaling ($\mathbf{G} = \begin{pmatrix} 1 & 0 \\ 0 & 1 \end{pmatrix}$); more precisely, the family of "balls," see text).

We may decompose $\boldsymbol{G}$ into quaternion-like elements (Lovejoy and Schertzer 1985; Schertzer and Lovejoy 1985b) :

$$\boldsymbol{G} = d\boldsymbol{I} + e\boldsymbol{I} + f\boldsymbol{J} + c\boldsymbol{K}$$

where

$$\boldsymbol{I} = \begin{pmatrix} 1 & 0 \\ 0 & 1 \end{pmatrix} \quad \boldsymbol{I} = \begin{pmatrix} 0 & -1 \\ 1 & 0 \end{pmatrix}$$
$$\boldsymbol{J} = \begin{pmatrix} 0 & 1 \\ 1 & 0 \end{pmatrix} \quad \boldsymbol{K} = \begin{pmatrix} 1 & 0 \\ 0 & -1 \end{pmatrix} \tag{8}$$

A fundamental parameter for the description of the overall type of anisotropy present in the system will be given by

$$a^2 = c^2 + f^2 - e^2 \tag{9}$$

In the case that $a^2 < 0$, we say that the system is rotation dominant: as the scale changes, the balls rotate through an infinite angle of rotation (although for a finite total scale ratio, only a finite amount of rotation is possible). If $a^2 > 0$, we call the system stratification dominant: in a like manner, an indefinitely large "stretching" of the unit ball is permitted, but the total amount of rotation never exceeds $\pi/2$.

Thus, an analysis of the anisotropies of our system involves determining the parameters c, d, f, and e, along with the spheroscale (or other family of balls). This completely determines the scaling anisotropy of the system in the approximation of linear GSI. For cases involving position-dependent anisotropy, the linear GSI approx-

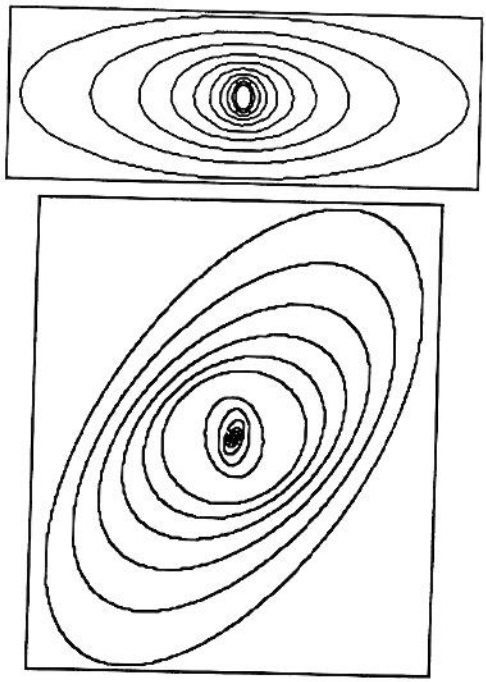

Figure 4 Top: Self-affine scaling with $\mathbf{G} = \begin{bmatrix} 1 & 0 \\ 0 & 5/9 \end{bmatrix}$ representing a vertical cross-section of the atmosphere. The shape of the balls models the average eddy shape; the flattening of the large balls models the fact that the atmosphere is increasingly stratified at large scale, and the small-scale vertically oriented balls correspond to "convective" type eddies or "rain shafts." The value 5/9 is that obtained from observations and theoretical arguments concerning the stratification of the horizontal wind (Schertzer and Lovejoy, 1985a). Bottom: More complex anisotropy (horizontal cross-section), with $\mathbf{G} = \begin{bmatrix} 1.25 & 0.75 \\ 1.25 & 0.75 \end{bmatrix}$. This shows the rotational effects of off-diagonal elements.

imation may be made over subregions of the system, as in the section, Cloud Radiances, below. Of course, this applies only to positive scalar fields; for problems involving continuum mechanics, an extension to vector and tensor multifractal fields is necessary (Schertzer and Lovejoy, 1995a).

DATA ANALYSIS

A full analysis for all the relevant parameters involves several techniques. Because of its sensitivity to scaling (and possible breaks thereof) and also because of its greater familiarity to geophysicists, one of the most basic analysis tools that we use to examine the scaling behavior of a system is a measurement of the power spectrum. The power spectrum, $E(k)$, at wave number $k = |\underline{k}|$ where $\underline{k}$ is the wave vector, is defined as the ensemble average of the angular integral of the square of

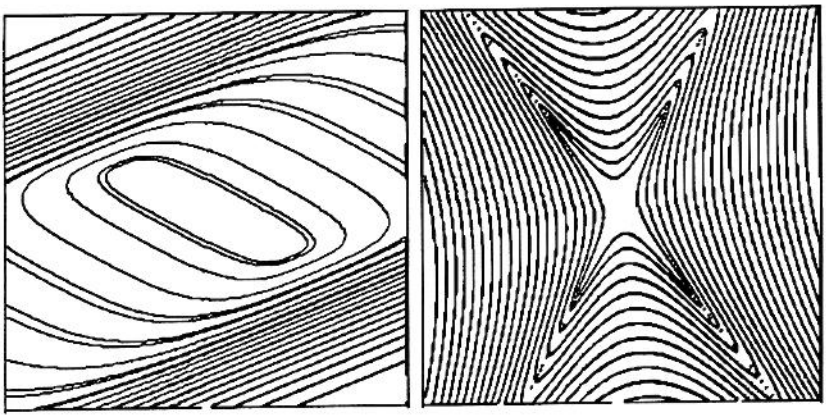

Figure 5 Fourth order polynomial balls, showing non-elliptical contours: on the left is a convex stratification dominant example, with $\mathbf{G} = \begin{bmatrix} 1.5 & 0.13 \\ 1.27 & 0.5 \end{bmatrix}$; on the right is a rotation dominant example showing highly non-convex shapes, with $\mathbf{G} = \begin{bmatrix} 1.1 & -0.1 \\ 0.3 & 0.9 \end{bmatrix}$.

the Fourier transformed field. In an isotropic scaling system we can express the $E(k)$ as:

$$E(k) \sim k^{-\beta} \tag{10}$$

This parameter, the "spectral slope," β, is useful for describing as well as simulating the process and is related to the moment scaling function by (Monin and Yaglom, 1975; Lavallée et al., 1993b)

$$\beta = 1 - K(2) + 2H \tag{11}$$

where $K(q)$ is the moment scaling function for the conservative process and H is the degree of non-conservation of the mean of the process. Thus, given the universal parameters α and C_1 we may determine $K(2)$ from Eq. 3 and hence the exponent H from the measured spectral slope.

To estimate α and C_1, it is often convenient to use a double trace moment technique (Lavallée, 1991; Lavallée et al., 1992). The field ε is renormalized by first raising its values at the finest resolution to the power η and then integrating (or degrading or dressing) up to a scale λ. This renormalized field will then be described by its own moment scaling function, $K(q, \eta)$. The relation between $K(q, \eta)$ and the usual statistical scaling exponent $K(q)$ is (Halsey, 1989; Lavallée et al., 1992):

$$K(q,\eta) = K(q\eta) - qK(\eta) \tag{12}$$

For the case where the process is a universal multifractal we have:

$$K(q,\eta) = \eta^{\alpha} K(q) = \eta^{\alpha} \cdot \frac{C_1}{\alpha - 1}\left(q^{\alpha} - q\right) \tag{13}$$

The scaling exponent in this case has two components: one depends on the universal parameter α only while the second is $K(q)$, the usual scaling exponent. By isolating the first component we can determine the value of the parameter α directly and then deduce C_1. By plotting $K(q, \eta)$ vs. η on a double logarithmic plot, we find the value of α from the slope of the line. Using this estimate of α and the value of q, we can deduce the value of C_1 from the intercept of the line with $\eta = 1$.

It must be noted, however, that in the case where $\beta > 1$, (i.e., where $H > 0$; see Eq. 3 and note that $K(2) > 0$) we cannot be dealing with a conserved process, and our estimates of α and C_1 will be inaccurate.[10] The field must be fractionally differentiated in order to yield a conserved process (i.e., it must be filtered by k^H in Fourier space in order to remove the effect of the fractional integration k^{-H}) and to obtain stable and accurate estimates of the multifractal parameters α and C_1 (see Lavallée et al., 1993b; Naud et al., 1996). In this case, however, to avoid technical complications with Fourier techniques (arising from the necessity of zero-padding our field and the associated numerical "ringing" this causes), the fractional differentiation in Fourier space was avoided. Instead, the modulus of the gradient of the fields was taken, having approximately the effect of a fractional differentiation of order 1. As long as $H < 1$, this is adequate for using the double trace moment (Lavallée et al., 1993b).

Strictly speaking the scaling exponents are determined from an ensemble average. It is necessary to have a large number of independent measurements of the field because of intermittency and the extreme variability of multifractal fields. Certain orders of singularity, corresponding to very high field values, may in fact have a codimension larger than the dimension of space, and will almost surely not appear in any given realization/example of the field. Nevertheless, these values will appear in a sufficiently large number of realizations and can be statistically important, even dominating the higher order statistical moments.[11]

SIMULATION

Once the multifractal parameters of the fields have been measured, we wish to simulate the type of geophysical field being studied, producing realizations of a stochastic anisotropic multifractal process. It should be emphasized that the aim of this is not to produce a facsimile of the fields analyzed; rather, it is to produce fields (each one a realization of the simulation process) of the same "type," i.e., with the same statistics — at all scales and intensitites — as the measured field (given by

[10] Specifically, there will be trivial scaling ($K = 0$) for all q below a critical (usually low) value.

[11] They will in fact generally cause a divergence of the high order moments of the field (Schertzer and Lovejoy, 1985a, 1987), associated with a non-classical form of self-organized criticality (Schertzer and Lovejoy, 1996). Thus, in order to obtain a full characterization of a field's multifractal parameters, we require a sufficiently large number of independent observations, so that the singularities corresponding to this critical moment of divergence q_D will appear.

$c(\gamma)$, which determines the probability distribution of field values — see Eq. 1). Since we use the framework of linear GSI, the anisotropic characteristics of the data will also be reproduced; this leads to realistic texture and morphology. In order to produce realizations that correspond to the measured parameters of our data, the technique of simulating continuous universal multifractal cascades was used (Schertzer and Lovejoy, 1987; Wilson et al., 1991; Pecknold et al., 1993). This simulation technique consists of generating an independent identically distributed Lévy noise,[12] with a Lévy index corresponding to the universal parameter α, and performing a fractional integration using an appropriate power-law filter function to produce a log-divergent generator (the logarithm of the field). This generator is then exponentiated, and the resulting multifractal field may then be "H-filtered" (i.e., fractionally integrated or differentiated by the order H to produce a non-conservative field, as explained above), in effect causing a scale-invariant "smoothing" or "roughening," respectively, of the field. For fields exhibiting scaling anisotropy, the filter function is modified to take into account non-isotropic notions of scale implied by the GSI parameters of the system being modeled. A graphical representation of the simulation procedure may be found in Plate 13*. This type of simulation was performed for all the data types analyzed, using the universal multifractal and GSI parameters determined. We may note that space/time realizations can be made by further modifications of the filter to ensure that causality is respected; see Marsan et al. (1996); Tessier et al. (1996).

DATA AND RESULTS

Landscape Topography

It has been known for almost half a century that topography has a power law spectrum over a wide range of scales (Venig-Meinesz, 1951), indicating scaling of at least the second-order moment. Indeed, topography has been a frequent subject of study by fractal analyses (see e.g., Goodchild, 1980; Aviles et al., 1987; Okubo and Aki, 1987; Turcotte, 1989; De Cola, 1990). However, since topography is better described as a scale-invariant field, rather than a scale-invariant geometric set of points, *a priori* there will be no unique fractal dimension for topography. Rather, each set exceeding a different altitude threshold will have its own fractal dimension, decreasing with increasing altitude threshold: it will be a multifractal field. Multifractal analyses of topography (Lovejoy and Schertzer, 1990; Lavallée et al., 1993b; Lovejoy et al., 1995) have convincingly confirmed this in several regions of the world.

To illustrate this, we analyzed the power spectra and the universal multifractal parameters of landscape topography. The power spectrum analysis used 20 contiguous 512 × 512 sections of U.S. topography data, from the area near latitude 40° N, and longitude 110° W, at a spacing of 3 arc seconds, corresponding to approxi-

[12] Lévy distributions are the result of the generalized central limit theorem for the sum of i.i.d. random variables; the Gaussian is the familiar special case, corresponding to $\alpha = 2$.

* Color plates follow numbered page 168.

mately 90-m resolution. An example of the data is shown in Plate 14*. The power spectrum of all 20 of these realizations of this data is shown in Figure 6; we note that this shows excellent scaling of $E(k)$ over the whole range of 2.5 orders of magnitude. The spectral slope is given by $\beta = 1.91$, in close agreement with the approximate value of $\beta \approx 2$ noted in the literature[13] (Venig-Meinesz, 1951; Bell, 1975).

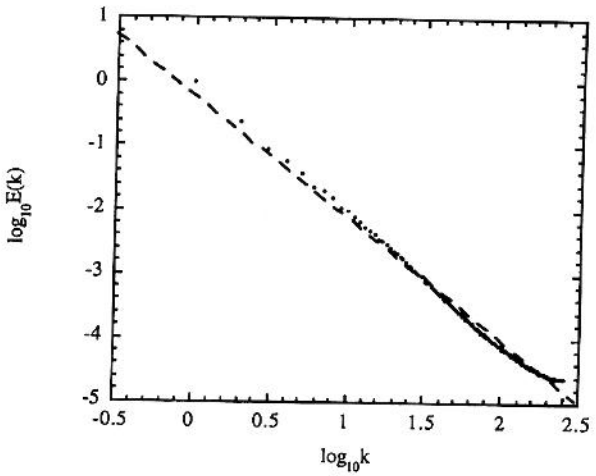

Figure 6 The power spectrum for 20 realizations of topography data. The spectral slope determined by linear regression is $\beta = 1.91$. Note the slight curvature at the large wavenumber end is probably associated with noise at the highest resolution of the data (corresponding to 2×9 m).

Having determined the spectral slope, it remains to find the multifractal parameters α and C_1. Because of the strong variability and intermittency of multifractal fields, analysis of data, as mentioned above in Data Analysis, is best performed on a large number of independent realizations. Indeed, because scaling is a statistical symmetry, on any individual realization the scaling is necessarily broken; the values obtained for α, C_1 and H will only be statistical estimates. Additionally, in order to estimate α, it is necessary to have good statistics for the lower order singularities of the field.[14] This can lead to difficulties, particularly in topography data. Regions of low gradient are generally sampled at a much lower resolution than highly variable areas, and this, in conjunction with quantization difficulties (this dataset, for example, has altitude measured only to the nearest meter) can result in large areas with an erroneous exactly zero gradient. Although the scaling for high $q \gtrsim 0.3$ were unaffected (since they are insensitive to the low gradients), the estimate of α is sensitive to the low q scaling and such artificially zero gradients, which can cause a significant decrease in the estimate of the parameter α (here, from the true value of $\alpha \approx 1.7$ to

[13] In Lovejoy and Schertzer (1995) it is shown how the value $\beta = 1.91$ can be accounted for via multifractal intermittency corrections to a basic $\beta = 2$ law.

[14] This is because α is the order of nonanalyticity of $K(q)$ at $q = 0$ (see Eq. 3) and the $q \approx 0$ statistics are dominated by the frequent low values of the gradients.

* Color plates follow numbered page 168.

about 1.35). In analyzing our dataset at the nominal 90-m resolution, it was noticed that up to 20% of our field was exactly zero gradient; accordingly, a 2048 × 2048 section was taken and coarse-grained to 256 × 256, giving a scale range of about 0.7 to 120 km. The data are currently being analyzed using a Fourier filtering technique to sidestep the problems given by such low gradients. Preliminary results correspond to those given here, and indicate that the need for coarse-graining will be obviated, allowing for the use of the entire scaling range of data.

An example of the multiscaling of the data is noted in Figure 7: the trace moment of the mean of various moments of the field (the trace moment is the average over the realizations of the η moments of the field, degraded to a scale ratio λ and then the q-th moment summed) shows excellent scaling (power-law behavior) of each moment over the entire range of data.

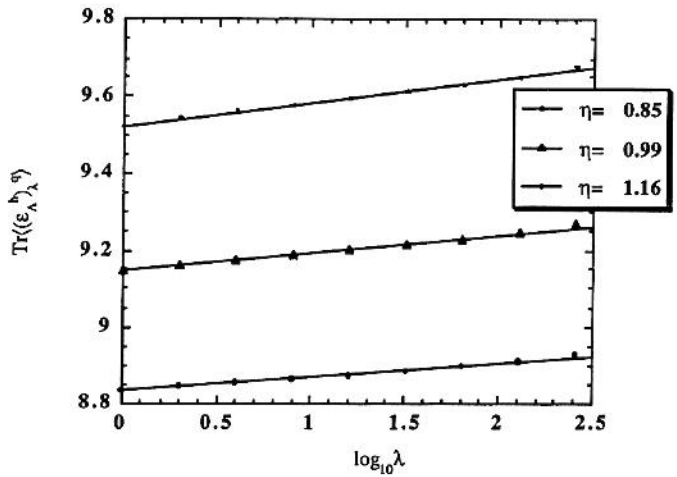

Figure 7 Scaling of the trace of the moments of topography data, for 3 different moments η, with $q = 1.5$. $\lambda = 1$ corresponds to 180 km.

A double trace moment analysis (defined in Data Analysis) of the data yielded the values $\alpha = 1.70 \pm 0.05$ and $C_1 = 0.07 \pm 0.01$; the $\log K(q,\eta)$ vs. $\log\eta$ curve is shown in Figure 8. A comparison of the moment scaling function of one section of the field with the theoretical $K(q)$ curve (see Eq. 3) is shown in Figure 9. The value for α is slightly lower than that found in a study of the topography of Deadman's Butte ($\alpha \approx 1.9$, from Lavallée et al., 1993b), but identical to that found from estimates of the universal multifractal parameters of the topography of France (see Table 1). These were for a single realization in each case. Analysis of data of the entire continental U.S. at 90-m resolution is proceeding. Together with the spectral slope, the parameters measured via double trace moment yield a value of $H = 0.52 \pm 0.05$, in close agreement with previously found values, as well as with theoretical arguments based on dimensional analysis (Lovejoy et al., 1995). We may note that this

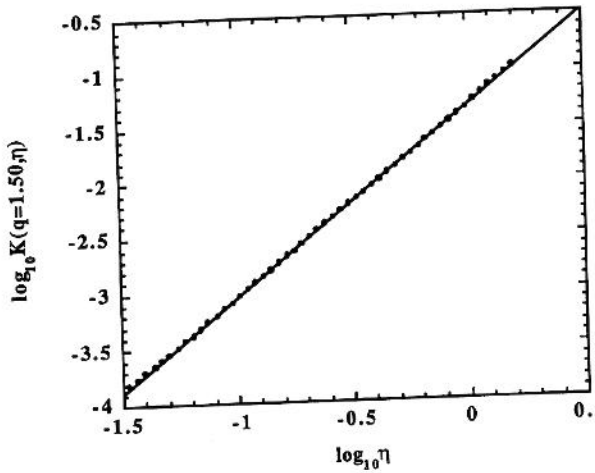

Figure 8 Graph of the double trace moment, $\log K(q,\eta)$ vs. $\log\eta$, for $q = 1.5$. The slope of the fit gives $\alpha = 1.70$, and its intercept gives $C_1 = 0.07$.

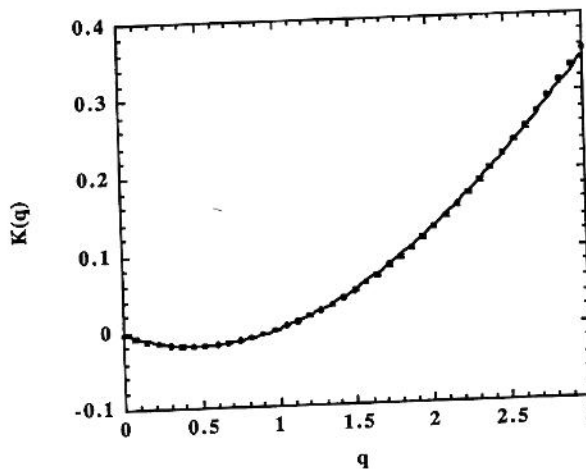

Figure 9 Comparison of theoretical moment scaling function with parameters determined from the double trace moment, with the measured scaling moment function of a degraded 256 × 256 section of topography data. The experimentally determined values are given by the circles. The curve is the theoretical value from Eq. 3, using $\alpha = 1.70$ and $C_1 = 0.07$. This clearly shows that the field is multifractal: a monofractal field would have a linear $K(q)$ function.

multifractal behavior rules out the popular self-affine surface models, since they are fundamentally monoscaling and thus have linear $K(q)$ curves.

Having found the universal multifractal parameters of our topography data, one of the sections was chosen for an analysis of its GSI parameters. It is pictured in

Plate 14* together with its spectral energy density, which shows the anisotropies in the system. In an isotropic system, the Fourier transform would have circular symmetry, rather than the roughly elliptical ones actually observed. This analysis was performed using the scale invariant generator (SIG) technique described in Lewis (1994). In SIG, an initial guess of the generator **G** is used to relate neighboring scales, and an error function based on the actual 2-D spectral density and the theoretically expected 2-D spectral density is defined, and a minimization over the GSI parameter space is performed to find the best fitting parameters c, f, and e. Here it was found that $c = 0.15, f = -0.10$, and $e = 0.41$, giving a rotation dominant system ($a^2 = -0.14$), with expected errors of roughly ± 0.05 on c and f, and ± 0.1 on e, which is a less well-estimated parameter (Lewis, 1994). Several examples, simulated using the values for multifractal and GSI parameters measured here but with different random seeds, are found in Figure 10. The difference between the realizations illustrates that any given examples using the same parameters have only the same statistics. A comparison of the 3-D ray-tracing representations of the realizations with that of the dataset reveals some resemblance at the larger scales. However, the flat regions that are seen at the smaller scales are not in general present in the simulated examples. It is suspected that this is caused by the erroneous areas of exactly zero gradient present in the data. Finally, not unexpectedly, the simulated realizations do not show river networks; algorithms to estimate the latter from the realizations exist and could perhaps yield even more visually realistic results.

Cloud Radiances

The multifractal nature of clouds must be taken into account when modeling their effects on the weather and climate (not to mention when dealing with their tendency to obscure surface phenomena in satellite imaging), and thus a good understanding of the statistical nature of cloud fields is important from a meteorological perspective. Beyond the importance of characterizing the basic variability via α, C_1 and H, GSI provides the attractive possibility of obtaining a quantitative basis for cloud classification, which is currently performed primarily by qualitative visual observation (or by operator assisted pattern recognition algorithms) on satellite data. This quantification may be regarded as a scaling extension of previous approaches involving measures of roughness and texture determined at a unique scale, or over a narrow range of scales. In contrast, GSI gives a measure of the latter over an arbitrarily large range of scales.

To illustrate this possibility, a set of analyses were performed on a series of visible channel satellite cloud images. These images were taken by the NOAA-9 satellite off the coast of Florida, longitude 70 West and latitude 27.5 North, during February 1986. The images analyzed were 512 × 512 pixel AVHRR channel 1, visible light images with wavelength 0.5 to 0.7 μm. The range of scales was 1.1 to 560 km.

These images were previously isotropically analyzed (Tessier et al., 1993) and shown to have good scaling, and universal multifractal parameters given by $\alpha = 1.13$

* Color plates follow numbered page 168.

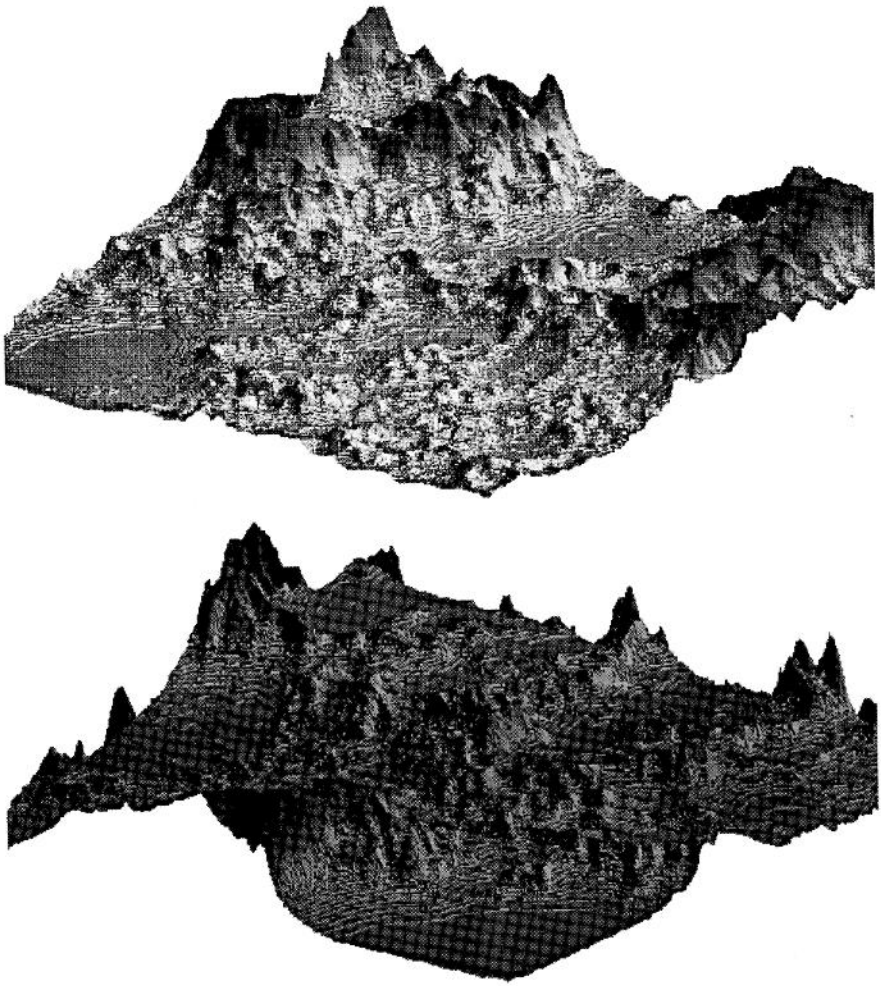

Figure 10 Four realizations of simulated landscape topography, using the parameters measured for the dataset $\alpha = 1.7$, $C_1 = 0.07$, $H = 0.5$, using different random seeds and incorporating anisotrophy using GSI parameters $c = 0.15$, $f = -0.10$, $e = 0.4$. They are visualized with ray-tracing techniques.

$\pm$ 0.20, $C_1 = 0.09 \pm 0.10$, and $H = 0.4 \pm 0.2$. An example of the scaling of the (isotropic) power spectrum of one of these images is given in Figure 11. The image, along with its spectral power density, is seen in Plate 15*. In a general cloud scene various cloud types coexist; this is an indication that we are dealing with non-linear (position-dependent) GSI. We therefore extracted from the original twelve images sixteen 256×256 pixel sub-images with fairly homogeneous cloud types (as determined by a professional meteorologist[15]) and analyzed their GSI parameters, working

[15] Dr. A. Bellon, McGill Weather Radar Observatory.

* Color plates follow numbered page 168.

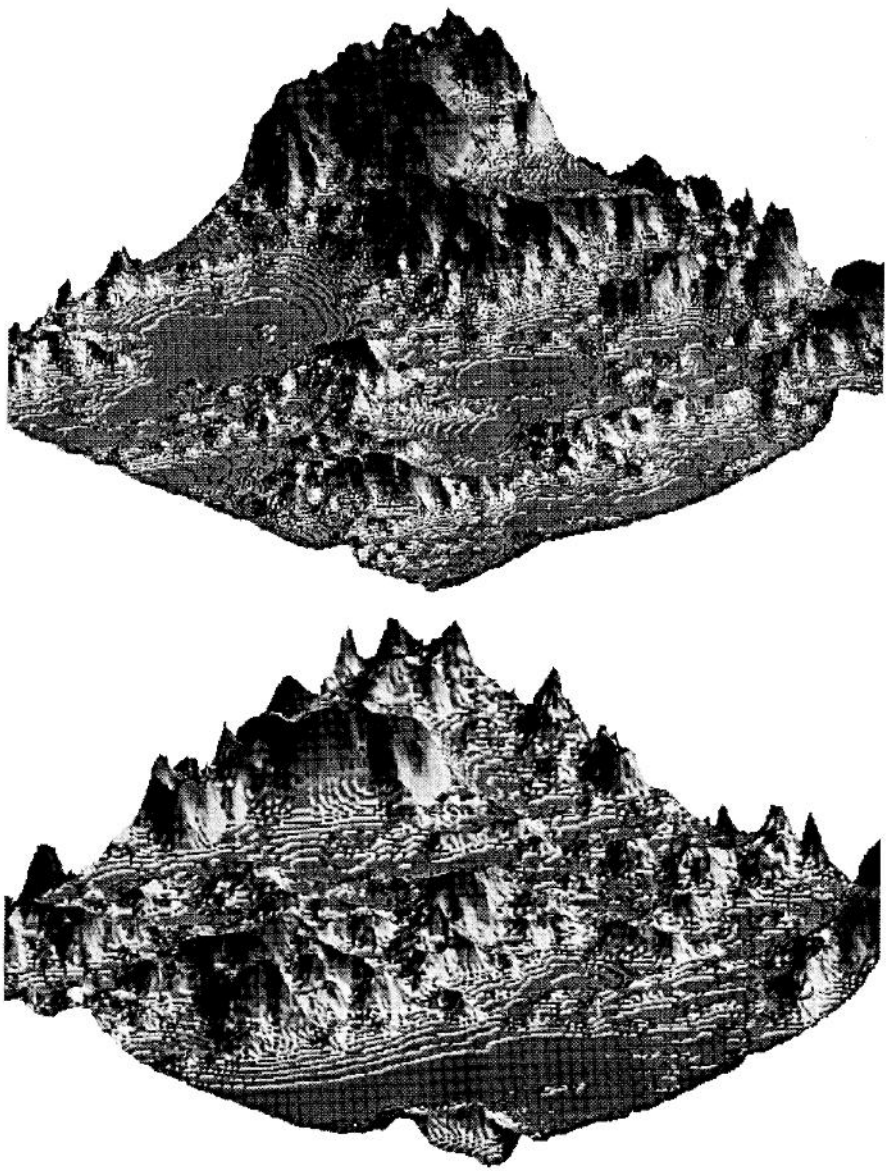

Figure 10 (continued)

under the hypothesis that various cloud types correspond to different linear approximations to GSI. The results are shown in Table 2.

Although considering the number of parameters measured, namely β, c, f, e, and the spheroscale, this is a small sample, we still see a clear clustering of parameters by cloud type; for example, the cumulus cases are all rotation dominant ($a^2 < 0$),

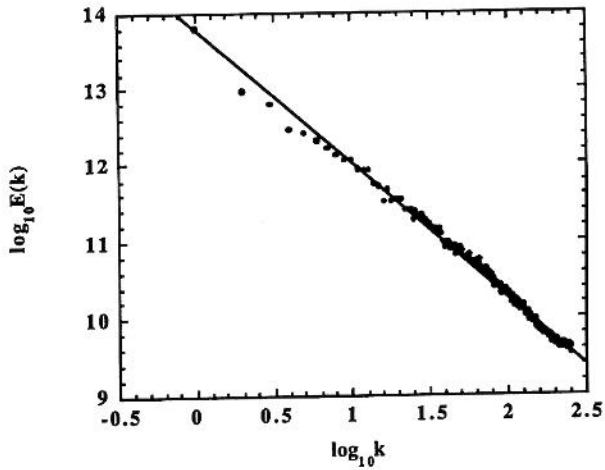

Figure 11 The power spectrum of a visible light cloud radiance field, wavelength 0.5 to 0.7 μm, range of scales 1.1 to 560 km. The spectral slope determined by linear regression is $\beta = 1.77$.

Table 2 Parameters of 16 subsections of NOAA-9 AVHRR channel 1 cloud radiance data, arranged by cloud type, giving β, the slope of the power spectrum, the GSI parameter *a*, and the size of the spheroscale. The parameter *a* is accurate to within ± 0.05 and $i^2 = -1$. The mesoscale convective complexes (MCC) were self-similar (isotropic) to within statistical error, so that any scale may be taken as a spheroscale

Stratification dominant clouds				Rotation dominant/isotropic clouds			
Cloud type	β	*a*	Spheroscale (km)	Cloud type	β	*a*	Spheroscale (km)
Cirrus	1.92	0.10	6.3	Cumulus	1.04	0.19*i*	34
Cirrus	1.77	0.65	10	Cumulus	1.21	0.05*i*	31
Cirrus	1.57	0.25	4.7	Cumulus	1.04	0.28*i*	28
Altocumulus	1.88	0.05	0.8	Stratus	1.79	0.0	2.3
Stratus	1.68	0.05	7.0	MCC	1.56	0.0	any
Stratus	1.65	0.05	2.9	MCC	1.83	0.0	any
Stratus	1.60	0.15	14				
Stratus	1.84	0.25	9.4				
Altostratus	1.91	0.10	9.4				
Nimbostratus	1.88	0.25	7.6				

with a comparatively large spheroscale.[16] Likewise, both examples of a mesoscale convective complex were nearly isotropic, while in general the cirrus clouds were more strongly stratification dominant than the stratus clouds (a^2 was larger). Simulated examples of cumulus and stratus types of cloud using some of the parameters given in Table 2 and the values for α, C_1 and H given above may be seen in Plates 16 and 17*. We may note that, comparing the simulated cumulus to the example

[16] Recall that the spheroscale is a scale at which structures are isotropic, and it need not exist. However, in all the cloud cases examined it was determined that a spheroscale could be approximately found at the scale indicated in Table 2, evidenced by the existence of a circular iso-energy contour in the 2-D spectral energy density.

* Color plates follow numbered page 168.

given, and likewise comparing the example of stratus cloud to that simulated, the general structures correspond rather well. Certain of the structures evident in the actual data are not present in the simulated examples. This is to be expected, since any given realization, actual or simulated, will not be identical to another. This large variability between different realizations of the same process is highlighted by the differences between the simulated clouds of each type, which were created using the same parameters. Still, the simulated cumulus consists, as does the real cumulus, of clusters of fairly small clouds arranged in bands. Likewise, the stratus example is a large scale complex consisting of a few fairly large, stratified structures, which can also be noted in the simulated stratus. It is obvious that the large parameter space involved in GSI requires that a large number of images of varying cloud types be analyzed to draw further conclusions.

It is also true that a complete classification and modeling scheme using GSI may have to take into account the properties of these cloud radiance fields not just in the visible spectrum, but also in the infrared, as indeed was necessary for qualitative visual classification. This is particularly true as regards the distinction between the lower altitude water clouds, such as cumulus and stratus, and the higher altitude ice clouds, cirrus. Currently, techniques are being developed for the analysis and modeling of vector multifractals (Schertzer and Lovejoy, 1995a), which should provide for a better understanding of the interrelations between different parts of the cloud radiance spectrum, as well as to provide more visually realistic simulated clouds. Indeed, it is naïve to expect a scalar multifractal framework (such as that presented here) to be completely adequate for studying clouds; the effect of the vector wind field is frequently apparent (e.g., in cyclones). The extension of linear GSI to nonlinear GSI may also allow for a greater ability to realistically describe these fields, allowing different types of basic anisotropy for different regions of the field.

A further application of the modeling of cloud systems currently being undertaken is the simulation of radiative transfer in multifractal clouds (for a 2-D version, see Davis et al., 1992; Naud et al., 1996; in 3-D, see Stanway et al., 1996). A 3-dimensional anisotropic cloud liquid water field is generated using the measured multifractal parameters (by the process described in Simulation), with a stratification in the vertical direction with respect to the horizontal (see Figure 12 for an image of the simulated cloud, and Figure 13 for the radiation field). Photons are then forward scattered through the cloud, using an isotropic phase function, with the intensity being estimated at the detector using spherical harmonics to help smooth out the high-frequency Monte Carlo noise. The resultant radiation fields may then be compared with satellite data. We are convinced that explicit cloud and radiation models of this type are essential for understanding cloud/radiation interactions (see also Davis et al., 1990; Gabriel et al., 1990; Lovejoy et al., 1990; Davis, 1992; Lovejoy and Schertzer, 1995; Naud et al., 1996 for more on radiative transfer in fractal and multifractal clouds).

Aeromagnetic Anomaly

The magnetic field of the Earth is a superposition of the main field internal to the planet, of fields arising from electrical currents flowing in the ionized upper

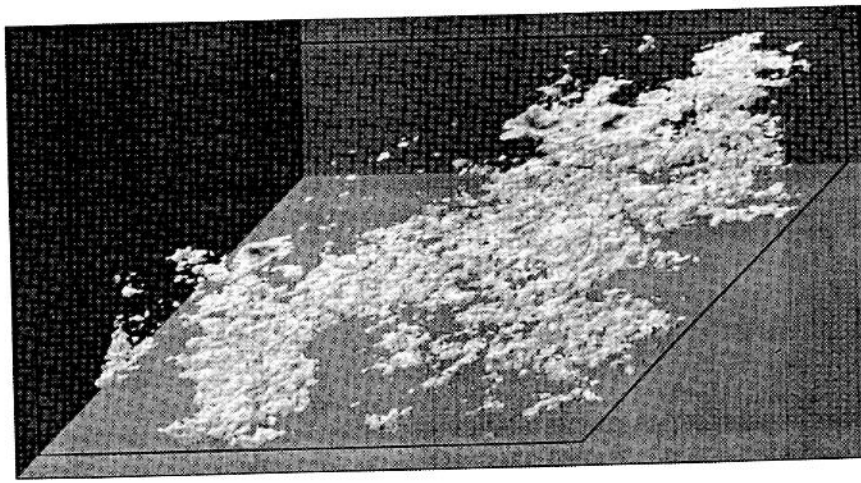

Figure 12 Three-dimensional multifractal cloud simulation, using universal multifractal parameters measured from satellite data. Only regions exceeding a minimum liquid water density are shown, the gray scale is proportional to the log of the density. The parameters are $\alpha = 1.35$, $C_1 = 0.10$, $H = 0.40$, and the vertical stratification is characterized by Hz = 0.55 (close to that for the wind field).

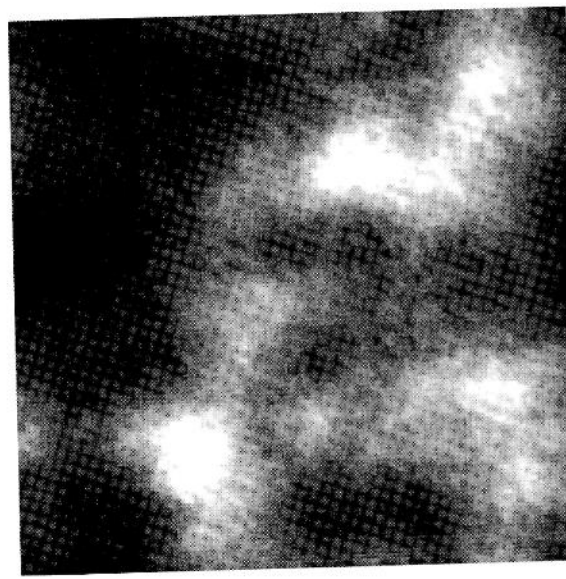

Figure 13 The results of Monte Carlo scattering of 150 000 000 photons through the cloud in Figure 12 with the mean optical thickness at the vertical as 1.0, seen from above. The sun was incident at 0.0 radians, with the results smoothed to partially remove the high-frequency Monte Carlo noise. Note that more realistic clouds would have highly forward-peaked phase functions.

atmosphere, and of fields induced by currents flowing within the Earth's crust. We analyzed airborne data of (the modules) of these magnetic fields, with the (transient)

atmospheric effects statistically removed (by a complex set of pre-processing filtering operations[17]). Seven data sets from varying regions of Canada were analyzed for their multifractal parameters. The aeromagnetic fields, whose properties are discussed in depth in Pecknold et al. (1996), were obtained on 256 × 256 (maximum) sized square grids which were coarse grained to 128 × 128 over an approximately 200 × 200 km area, yielding a maximum resolution of ~1.6 km (see Plate 18* for an example). The coarse graining was performed to eliminate significant artifacts at the highest frequencies, due most likely to the limited resolution of the measuring device, oversampling, or noise. Additionally, as can be seen from the power spectrum of the data (Figure 14), a fairly sharp break in the scaling occurs at about 10 km. This is believed to be caused by a high-pass filter used in the pre-processing to remove the transients as mentioned above. Below we study the multifractal behavior only over the range of scales in the high frequency regime.

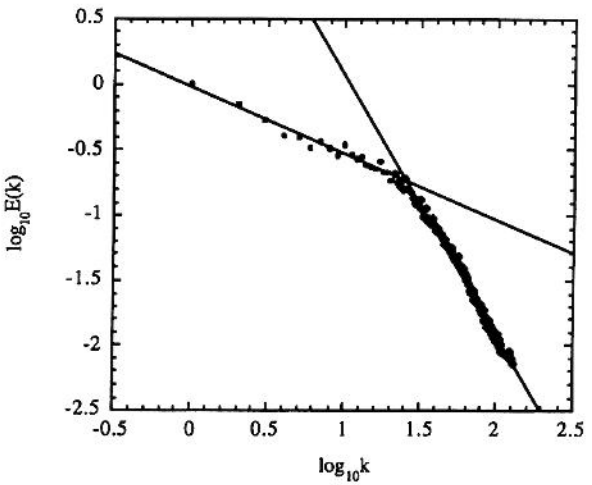

Figure 14 The power spectrum of seven aeromagnetic anomaly fields. The spectral slope for high frequencies is $\beta \approx 2.0$; for low frequencies $\beta = 0.53$. The relative flatness of the low frequency regime is believed to be an artifact of the data pre-processing to remove transients.

The universal multifractal parameters of the aeromagnetic field were measured (Pecknold et al., 1996) as $\alpha \approx 1.9 \pm 0.1$, $C_1 \approx 0.10 \pm 0.02$, and $H = 0.70$. An analysis of the GSI parameters for one of the datasets was performed (latitude 87° W, longitude 50° N) yielding values of $c = 0.05$, $f = 0.10$, $e = 0.22$, a rotation dominant system. In this dataset, however, no spheroscale appears to exist (this is confirmed by statistical analysis). We may see this by looking at the spectral energy density in Plate 18*: the shapes of the balls describing the anisotropy in this dataset are somewhat rhomboid-like (this may be seen best towards the center of the image, since the larger spectral density contours, corresponding to small-scale structures,

[17] Using proprietary software.

* Color plates follow numbered page 168.

are fairly noisy). The system was found to be reasonably well described by a family of fourth order polynomial balls, as described in Pecknold et al. (1996); the simple quadratic family of ellipses is insufficient to describe this system. The aeromagnetic field was simulated using the GSI and universal multifractal parameters measured for this dataset, and this is also shown in Plate 18. The general structure is seen to be quite similar to that of the dataset.

Sea Ice

Finally, the radar reflectivity of sea ice was examined. Recent work has shown scaling of synthetic aperture radar reflectivity fields of sea ice over almost three orders of magnitude (Falco et al., 1996), and found multifractal statistics over the range of ~12 m to 6 km. These multifractal parameters and the GSI parameters of two different scenes of SAR reflectivity fields from sea ice, in several wavelength and polarization combinations, were estimated. The fields were 512 × 512 pixels, with a resolution of 12.5 m. The measurements were by the Jet Propulsion Laboratory airborne SAR operating simultaneously at the C band (5.6 cm) and L band (25 cm) wavelength ranges, transmitting and receiving from separate antennas in three linear polarization combinations: HH, VV, HV, where the symbols represent horizontal (H) and vertical (V) polarizations in the transmitted and received beams respectively. The data images were taken from an altitude of 9 km over the Beaufort Sea (76° N – 165° W) in March 1988 (Drinkwater et al., 1991). One of the images analyzed is shown in Plate 19*. In the image, ridges, lees and ice types of various ages can be identified. The scaling of the power spectrum of this example is shown in Figure 15, giving a spectral slope of $\beta = 0.83$. In some cases, the scaling of the power spectrum is affected by the large anisotropies present in the system. The universal multifractal parameters for sea ice were given by $\alpha = 1.85 \pm 0.05$, $C_1 = 0.01 \pm 0.01$, and $H = -0.05$ to -0.15, with only the value of H varying with polarization and wavelength.

The GSI parameters were not very sensitive to the polarizations, but did vary from scene to scene. In the case of our image, the parameters were found to be $c = 0.21$, $f = 0.0$, and $e = 0.0$. This field was also analyzed for its unit ball, and it was found that it was best described, as in the case of the aeromagnetic anomaly dataset, by fourth order polynomials. In fact, the original aim of extending the simplest case of linear GSI, described by elliptical families of balls, to the families of quartic balls, was to provide a description of the ridges, fissures and lees present in SAR ice images (Pecknold et al., 1996). These structures do not seem to be adequately modeled by the framework of linear GSI with a spheroscale, since they have pronounced nonconvex Fourier space isolines (corresponding to the balls; see e.g., Figure 5 above). A simulated sea ice field made using the parameters given above is found in Plate 20*. We note that the large scale structures, in particular the floes and fissures, are not reproduced, although some degree of clustering into larger scale structures may be noted, as well as certain aspects of the texture. We suspect that

* Color plates follow numbered page 168.

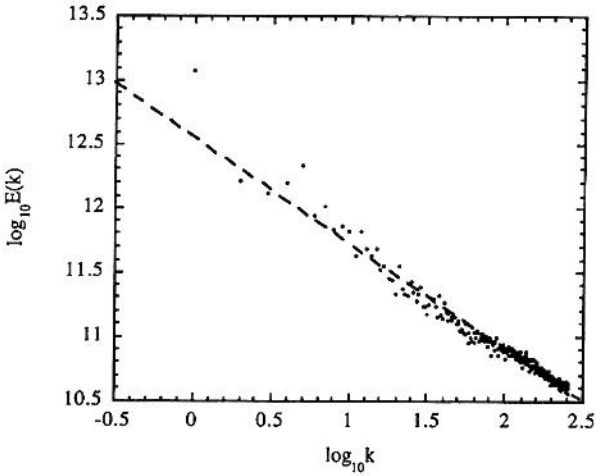

Figure 15 The power spectrum of a sea ice radar reflectivity field. The spectral slope determined by linear regression is $\beta = 0.83$.

use of tensor, rather than scalar, multifractals may lead to significant improvement since the ice field is determined largely by stress and strain tensors.

SUMMARY

The quest for more realistic ways to represent and model geographical and geophysical systems, together with the fact that most remotely sensed fields exhibit scaling over the physically significant ranges, has led to the recognition that multifractals are a fundamental theoretical tool. The framework of scalar universal multifractals, together with linear generalized scale invariance, permits fairly realistic modeling both of the statistical properties and of the visual characteristics of many geographically and geophysically significant fields. It does this with only six basic exponents — three describing the infinity of fractal dimensions, and another three describing the anisotropy (and therefore texture and morphology) over the entire scaling range. We have a relatively simple yet surprisingly realistic description of the field — and of its aggregation/resolution dependent properties — over arbitrarily wide ranges of scales. In comparison, standard modeling techniques start from approximate non-linear deterministic partial differential equations and then seek to integrate these over a numerically manageable range of scales, typically only about two orders of magnitude. They necessarily make unrealistic homogeneity assumptions about the unresolved scales which can in fact result in a feedback of large uncontrollable errors on the resolved scales.[18] Even when this is accomplished they still give no information about how the results can be extended to smaller (or larger) scales. The main extensions of the multifractal framework which will be necessary

[18] These assumptions go under the general rubric of "parameterization"; the existence of self-organized critical (small scale) fluctuations generally predicted by multifractal cascade theory indicates that such deterministic parameterizations cannot generally succeed.

are from scalar to vector and tensor multifractals (and their more complex universality classes), and from linear GSI (position independent) to a full non-linear (position dependent) version. In short, it is easy — without leaving the general scaling multifractal framework — to introduce more parameters and increase realism.

Further work is still necessary to obtain a more accurate and comprehensive picture of the place of universal multifractals and GSI in the study of geographical and geophysical systems. For example, the analysis of GSI parameters of clouds to determine the relationship between this anisotropic parameterization and the cloud classification is ongoing. Likewise, the problem of recognition of sea ice may be examined by relating its anisotropies to its morphology, and an analysis of aeromagnetic anomalies may provide some clues as to the underlying structure and composition of the Earth's crust.

More complete analysis of available topography data will also be performed. Currently, the entire continental U.S. at a resolution of 3″ of arc is being analyzed for scaling and for its multifractal parameters. Preliminary estimates of the topography of the Earth at a resolution of 5′ are also continuing, and show consistency with the results obtained thus far for smaller data sets.

Finally, new methods are being developed for analysis and modeling, such as techniques for analyzing and simulating multifractal fields on a sphere, a necessity in conjunction with the extension of global data (see Plate 21* for an example of simulated topography on the sphere, Tan et al., 1996). Additionally, methods dealing with vector and tensor fields ("Lie cascades," Schertzer and Lovejoy, 1995a) promise to provide further insight into the more complicated physics that underlies the systems that we observe. The present techniques of multifractal modeling, dealing as they do with scalar fields and cascades of scalar quantities, are insufficient to deal completely with interrelated fields such as the multiple channel satellite-imaged cloud radiance fields. Likewise, dealing with vector fields such as velocity fields also suggests the need for further developments in the modeling of multifractals. Thus, this framework of Lie cascades provides hope for yet more realistic and accurate modeling of the world around us.

REFERENCES

Adelfang, S. I., On the relation between wind shears over various intervals. *J. Atmos. Sci.*, 10, 138, 1971.

Aviles, C. A., Scholz, C. H., and Boatwright, J., Fractal analysis applied to characteristic segments of San Andreas fault, *J. Geophys. Res.*, 92, 331, 1987.

Bak, P., Tang, C., and Weiessenfeld, K., Self-organized criticality: An explanation of 1/f noise, *Phys. Rev. Lett.*, 59, 381, 1987.

Bell, T. H., Statistical features of sea floor topography, *Deep Sea Res.*, 22, 883, 1975.

Brosamlen, G., Multifractal analysis of cloud liquid water over the range 5m to 330km: a new test of the unified scaling model, M.Sc. thesis, McGill University, 1993.

* Color plates follow numbered page 168.

Chigirinskaya, Y., Schertzer, D., Lovejoy, S., Lazarev, A., and Ordanovich, A., Unified multifractal atmospheric dynamics tested in the tropics part 1: horizontal scaling and self-organized criticality. *Nonlin. Processes Geophys.*, (1), 105, 1994.

Davis, A., Lovejoy, S. and Schertzer, D., Supercomputer simulation of radiative transfer inside multifractal cloud models, in *I.R.S. 92*, Arkin, A., Lenoble, C., and Gelyn, J. F., Eds., Deepak, Hampton, VA, 112, 1992.

Davis, A., Lovejoy, S., Gabriel, P., Schertzer, D., and Austin, G. L., Discrete angle radiative transfer. Part III: numerical results on homogeneous and fractal clouds, *J. Geophys. Res.*, 95, 11729, 1990.

Davis, A., Marshak, A., Wiscombe, W., and Cahalan, R., Multifractalcharacterization of nonstationarity and intermittency in geophysical fields: observed, retrieved or simulated. *J. Geophys. Res.*, 99, 8055, 1994.

Davis, A., Radiation Transport in Scale Invariant Optical Media, Ph. D. thesis, McGill University, 1992.

Davis, F. and Simonett, D. S., GIS and remote sensing, *Geographic Information Systems*, Maguire, D. J., Goodchild, M. F. and Rhind, D. W., Eds., Longman Scientific and Technical Press, Harlow, UK, 1991, 191.

De Cola, L. and Lam, N., Introduction to fractals in geography, in *Fractals in Geography*, De Cola, L. and Lam, N., Eds., Prentice Hall, Englewood Cliffs, NJ, 1993.

De Cola, L., Fractal analysis of a classified LANDSAT scene, preprint, 1990.

Drinkwater, M. R., Kwok, R., Winnebrenner, D. P., and Rignot, E., Multifrequency polarimetric SAR observations of sea ice, *J. Geophys. Res.*, 96, 20679, 1991

Endlich, R. M., and Mancuso, R. L., Objective Analysis of environmental conditions associated with severe thunderstorms and tornadoes. *Mon. Weather Rev.*, 96, 342, 1968.

Falco, T., Francis, F., Lovejoy, S., Schertzer, D., Kerman, B., and Drinkwater, M., Scale invariance and universal multifractals in sea ice synthetic aperature radar reflectivity fields, IEEE Trans, *Geosci. Remote Sensing*, 34, 906, 1996.

Frisch, U. P., Sulem, P. L. and Nelkin, M., A simple dynamical model of intermittency in fully developed turbulence, *J. Fluid Mech.*, 87, 719, 1978.

Gabriel, P., Lovejoy, S., Davis, A., Schertzer, D. and Austin, G. L., Discrete angle radiative transfer. Part II: renormalization approach to scaling clouds, *J. Geophys. Res.*, 95, 11717, 1990.

Garrido, P., Lovejoy, S., and Schertzer, D., Multifractal processes and self-organized criticality in the large scale structure of the universe, *Physica A*, 225, 294, 1996.

Goodchild, M. F., Fractals and the accuracy of geographical measures, *Math. Geol.*, 12, 85, 1980.

Grassberger, P., Generalized dimensions of strange attractors, *Phys. Rev. Lett.*, A 97, 227, 1983.

Halsey, T. C., Multifractality, scaling and diffusive growth, in *Fractals Physical Origin and Properties*, Pietronero, L., Ed., Plenum Press, New York, 1989.

Halsey, T. C., Jensen, M. H., Kadanoff, L. P., Procaccia, I. and Shraiman, B., Fractal measures and their singularities: the characterization of strange sets, *Phys. Rev. A*, 33, 1141, 1986.

Hentschel, H. G. E. and Procaccia, I., The infinite number of generalized dimensions of fractals and strange attractors, *Physica D*, 8, 435, 1983.

Hooge, C., Earthquakes as a Space-Time Multifractal Process. M.Sc. thesis, McGill University, 1993.

Hooge, C., Lovejoy, S., Schertzer, D., Pecknold, S., Malouin, J.-F., and Schmitt, F., Multifractal phase transitions: the origin of self-organized criticality in earthquakes. *Nonlin. Processes Geophys.*, 1(2), 191-197, 1994.

Hubert, P., Tessier, Y., Ladoy, P., Lovejoy, S., Schertzer, D., Carbonnel, J. P., Violette, S., Desurosne, I., and Schmitt, F., Multifractals and extreme rainfall events. *Geophys. Res. Let.*, 20(10), 931, 1993.

Kapteyn, J. C., Skew frequency curves in biology and statistics, *Publ. Astron. Lab. Groningen*, 1903.

Ladoy, P., Schmitt, F., Schertzer, D., and Lovejoy, S., Analyse multifractale de la variabilité temporelle des observations pluviometrique à Nimes. Comptes Rendus de l'Académie des Sciences de Paris, II(317), 775, 1993.

Larnder, C., Desaulnier-Soucy, N., Lovejoy, S., and Schertzer, D., Evidence for universal multifractal behaviour in human speech. International Journal of Chaos and Bifurcation, 2(3), 715, 1992.

Lavallée, D., Multifractal techniques: Analysis and Simulation of Turbulent Fields, Ph.D. thesis, McGill University, 1991.

Lavallée, D., Jourdan, D., Gautier, C., and Hooge, C., Universal multifractal properties of microwave satellite data, *ASPRS/ACSM 1993, Annual Convention and Exposition, New Orleans*, 1993a.

Lavallée, D., Lovejoy, S., Schertzer, D., and Ladoy, P., Nonlinear variability and landscape topography: analysis and simulation, in *Fractals in Geography*, De Cola, L. and Lam, N., Eds., Prentice-Hall, Englewood Cliffs, NJ, 1993b, 171.

Lavallée, D., Lovejoy, S., Schertzer, D., and Schmitt, F., On the determination of universal multifractal parameters in turbulence, *Topological Aspects of the Dynamics of Fluids and Plasmas*, Moffat, K., Tabor, M. and Zalslavsky, G., Eds., Kluwer, Boston, 1992, 463.

Lazarev, A., Schertzer, D., Lovejoy, S., and Chigirinskaya, Y., Unified multifractal atmospheric dynamics tested in the tropics part II: vertical scaling and generalized scale invariance. *Nonlin. Processes Geophys.*, 1, 115, 1994.

Lewis, G., The Scale Invariant Generator Technique and Scaling Anisotropy in Geophysics, M.Sc. thesis, McGill University, 1994.

Lovejoy, S., Gabriel, P., Davis, A., Schertzer, D., and Austin, G. L., Discrete angle radiative transfer. Part I: scaling and similarity, universality and diffusion, *J. Geophys. Res.*, 95, 11699, 1990.

Lovejoy, S., Lavallée, D., Schertzer, D., and Ladoy, P., The $l^{1/2}$ law and multifractal topography: theory and analysis, *Nonlin. Process. Geophys.*, 2, 16, 1995.

Lovejoy, S. and Schertzer, D., Generalized scale invariance in the atmosphere and fractal models of rain, *Water Resour. Res.*, 21(8), 1233, 1985.

Lovejoy, S. and Schertzer, D., How bright is the coast of Brittany?, in *Fractals in Geoscience and Remote Sensing*, Wilkinson, G., Kanellopoulos, I. and Mégier, J., Eds., Office for Official Publications of the European Communities, Luxembourg. 1, 1995, 102.

Lovejoy, S. and Schertzer, D., Our multifractal atmosphere: a unique laboratory for non-linear dynamics, *Phys. Can.*, 46, 62, 1990.

Lovejoy, S. and Schertzer, D., Scale invariance in climatological temperatures and the spectral plateau. *Ann. Geophys.*, 4B, 401, 1986.

Mandelbrot, B. B., How long is the coastline of Britain? Statistical self-similarity and fractional dimension, *Science*, 155, 636, 1967.

Mandelbrot, B. B., Intermittent turbulence in self-similar cascades: divergence of high moments and dimension of the carrier, *J. Fluid Mech.*, 62, 331, 1974.

Mandelbrot, B. B., Negative dimensions and Hölders, multifractals and their Hölder spectra, and the role of lateral preasymptotics in science, *J. Fourier Anal. Appl.* (Kahane Special Issue), 1995.

Mandelbrot, B. B., Stochastic models for the Earth's relief, the shape and the fractal dimension of the coastlines, and the number-area rule for islands, *Proc. Nat. Acad. Sci. U.S.A.*, 72, 3825, 1975.

Marsan, D., Schertzer, D., and Lovejoy, S., Causal space-time multifractal processes: predictability and forecasting of rain fields, *J. Geophys. Res.*, (in press), 1996.

Marsan, D., Schertzer, D. and Lovejoy, S., Causal space-time multifractal modelling of rain, *J. Geophys Res.*, (in press), 1996.

Meneveau, C. and Sreenivasan, K. R., Simple multifractal cascade model for fully developed turbulence, *Phys. Rev. Lett.*, 59(13), 1424, 1987.

Monin, A. S. and Yaglom, A. M., *Statistical Fluid Mechanios*, MIT Press, Boston, 1975.

Naud, C., Schertzer, D., and Lovejoy, S., Fractional integration and radiative transfer in multifractal atmospheres, in *Stochastic Models in Geosystems*, Molchanov, S. and Woyczynski, W., Eds., Springer-Verlag, New York, 1996, 239.

Nguyen, V. T. V., Pandley, G. R., and Rousselle, J., Estimation of missing short-duration rainfalls using data measured at longer time scales, in *6th International Conference on Urban Storm Drainage*, Marsalek J. and Torno H. C., Eds., Niagara Falls, Ontario, Canada, 1993, 170.

Novikov, E. A. and Stewart, R., Intermittency of turbulence and spectrum of fluctuations in energy-dissipation, *Izv. Akad. Nauk. SSSR. Ser. Geofiz.*, 3, 408, 1964.

O'Brien, L., *Introducing Quantitative Geography: Measurement, Methods, and Generalised Linear Models*, Routledge, London; New York, 1992.

Okubo, P. G. and Aki, K., Fractal geometry in the San Andreas fault system, *J. Geophys. Res.*, 92, 345, 1987.

Olsson, J., Niemczynowicz, J., and Berndtsson, R., Limits and characteristics of the multifractal behavior of a high-resolution rainfall time series. *Nonlin. Processes Geophys.*, 2(1), 23, 1995.

Parisi, G. and Frisch, U., A multifractal model of intermittency, *in Turbulence and Predictability in Geophysical Fluid Dynamics and Climate Dynamics*, Ghil, M., Benzi, R. and Parisi, G., Eds., North Holland, Amsterdam, 1985, 84.

Pecknold, S., Lovejoy, S., and Schertzer, D., The morphology and texture of anisotropic multifractals using generalized scale invariance, in *Stochastic Models in Geosystems*, Molchanov, S. and Woyczynski, W., Eds., Springer-Verlag, New York, 1996, 269.

Pecknold, S., Lovejoy, S., Schertzer, D., and Hooge, C., Universal multifractals and anisotropic scale invariance in aeromagnetic fields, *Geophys. Int. J.*, (in preparation), 1996.

Pecknold, S., Lovejoy, S., Schertzer, D., Hooge, C., and Malouin, J.-F., The simulation of universal multifractals, in *Cellular Automata: Prospects in Astrophysical Applications*, Lejeune, A. and Perdang, J., Eds., World Scientific, Singapore, 1993, 228.

Perrin, J., *Les Atomes*, NRF-Gallimard, Paris, 1913.

Richardson, L. F., *Weather Prediction by Numerical Process*, Cambridge University Press, 1922, Republished by Dover, New York, 1965.

Richardson, L. F., The problem of contiguity: an appendix of statistics of deadly quarrels, *Gen. Syst. Yearb.*, 6, 139, 1961.

Schertzer, D. and Lovejoy, S., The dimension and intermittency of atmospheric dynamics, *Turbulent Shear Flows 4*, University of Karlsruhe, Karlsruhe, FRG, Springer-Verlag, 1983.

Schertzer, D. and Lovejoy, S., The dimension and intermittency of atmospheric dynamics, *Turbulent Shear Flows 4*, Launder, B., Ed., Springer, 1985a, 7.

Schertzer, D. and Lovejoy, S., Generalised scale invariance in turbulent phenomena, *Physico-Chem. Hydrodynam. J.*, 6, 623, 1985b.

Schertzer, D. and Lovejoy, S., Physical modeling and analysis of rain and clouds by anisotropic scaling of multiplicative processes, *J. Geophys. Res.*, D 8(8), 9693, 1987.

Schertzer, D. and Lovejoy, S., Generalized scale invariance and multiplicative processes in the atmosphere, *PAGEOPH*, 130, 57, 1989.

Schertzer, D. and Lovejoy, S., Nonlinear geodynamical variability: multiple singularities, universality and observables, *Non-Linear Variability in Geophysics: Scaling and Fractals*, Schertzer, D. and Lovejoy, S., Eds., Kluwer, Boston, 1991a, 41.

Schertzer, D. and Lovejoy, S., Scaling nonlinear variability in geodynamics, in *Nonlinear Variability in Geophysics: Scaling and Fractals*, Schertzer, D. and Lovejoy, S., Eds., Kluwer Academic Publishers, Dordrecht, 41, 1991b.

Schertzer, D. and Lovejoy, S., Multifractal generation of self-organized criticality, in *Proceedings of the Second IFIP Working Conference on Fractals in the Natural and Applied Sciences*, Novak, M. M., Ed., North Holland, Amsterdam, 1994, 325.

Schertzer, D. and Lovejoy, S., From scalar cascades to Lie cascades: joint multifractal analysis of rain and cloud processes, in *Space/Time Variability and Interdependance for Various Hydrological Processes*, Feddes, R. A., Ed., Cambridge University Press, New York, 1995a.

Schertzer, D., and S. Lovejoy, Standard and advanced multifractal techniques for remote sensing, in *Fractals in Geoscience and Remote Sensing*, edited by Wilkinson, I.K.G., Mégier, J., Eds., Office for Official Publications of the European Communities, Luxembourg, 1995b, 11.

Schertzer, D. and Lovejoy, S., The multifractal phase transition route to self-organized criticality, *Phys. Rep.*, (in press), 1996.

Schertzer, D., and Lovejoy, S., Universal multifractals do exist!, *J. Appl. Meteorol.*, (in press), 1996b.

Schertzer, D., Lovejoy, S., Lavallée, D., and Schmitt, F., Universal hard multifractal turbulence: theory and observation, in *Nonlinear Dynamics of Structures*, Sagdeev, R. Z., Frisch, U., Moiseev, A. S., and Erokhin, A., Eds., World Scientific, Singapore, 1991, 213.

Schmitt, F., Lavallée, D., Schertzer, D., and Lovejoy, S., Empirical determination of universal multifractal exponents in turbulent velocity fields. *Phys. Rev. Let.*, 68, 305, 1992a.

Schmitt, F., Lovejoy, S., and Schertzer, D., Multifractal analysis of the Greenland ice-core project climate data. *Geophys. Res. Let.*, 22, 1689, 1995.

Schmitt, F., Lovejoy, S., Schertzer, D., Lavallée, D., and Hooge, C., First estimates of multifractal indices for velocity and temperature fields. Comptes Rendus de l'Académie des Sciences de Paris, serie II, 314, 749, 1992b.

Schmitt, F., Schertzer, D., Lovejoy, S., and Brunet, Y., Estimation of universal multifractal indices for atmospheric turbulent velocity data, *Fractals*, 3, 568, 1994.

She, Z.-S. and Waymire, E. C., Quantized energy cascade and log-poisson statistics in fully developed turbulence, *Phys. Rev. Lett.*, 74(2), 262, 1995.

Stanway, J. D., Lovejoy, S., and Pecknold, S., Monte Carlo simulation of radiative transfer in multifractal clouds, (in preparation), 1996.

Steinhaus, H., Length, shape and area, *Colloq. Math.*, III, 1, 1954.

Tan, J., Pecknold, S., Lovejoy, S., Schertzer, D., and Malouin, J. F., Simulations of continuous multifractal processes on the sphere, (in preparation), 1996.

Tessier, Y., Multifractal Objective Analysis, Rain and Clouds. Ph. D., McGill University, 1993.

Tessier, Y., Claerdebout, M., Lovejoy, S., Novak, R., Roff, J., Ingram, G., Bourget, E., and Schertzer, D., Universal multifractal analysis of plankton and related physical variables gathered during the CHASE experiment. *J. Mar. Ecol.*, (in preparation), 1996a.

Tessier, Y., Lataille, S., Lovejoy, S., and Schertzer, D., Multifractal analysis of the vegetation cover, in *EGS XX General Assembly*, Hamburg, Germany, 1995b.

Tessier, Y., Lovejoy, S., and Schertzer, D., Universal Multifractals: theory and observations for rain and clouds. *J. Appl. Meteorol.*, 32(2), 223, 1993b.

Tessier, Y., Lovejoy, S., and Schertzer, D., Multifractal analysis and simulation of the global raingage network. *J. Appl. Meteorol.*, 33, 1572, 1994.

Tessier, Y., Lovejoy, S., Schertzer, D., Hubert, P., and Pecknold, S., Multifractal analysis and modeling of rainfall and river flows and scaling transfer functions, *J. Geophys. Res.*, (in press), 1996c.

Tessier, Y., Lovejoy, S., Schertzer, D., Lavallée, D., and Kerman, B., Universal multifractal indices for the ocean surface at far red wavelengths. *Geophys. Res. Let.*, 20, 1167, 1993c.

Tessier, Y., Lovejoy, S., Schertzer, D., and Claerdeboudt, M., Scale invariant algorithms for remote sensing of ocean colour, *Int. J. Remote Sensing*, (in preparation), 1996b.

Tessier, Y., Lovejoy, S., Hubert, P., Schertzer, D., and Pecknold, S., Multifractal analysis and modeling of Rainfall and river flows and scaling, causal transfer functions, *J. Geophys. Res.*, (in press), 1996c.

Tessier, Y., Schertzer, D., and Lovejoy, S., The multifractal global raingage network: analysis and simulations, *J. Appl. Meteorol.*, 32(12), 1572, 1994.

Turcotte, D. L., Fractals in geology and geophysics, *Pageoph*, 131, 171, 1989.

Venig-Meinesz, F. A. (1951), A remarkable feature of the Earth's topography, *Proc. K. Ned. Akad. Wet. Ser. B Phys. Sci.*, 54, 212, 1991.

Wilson, J., Schertzer, D., and Lovejoy, S., Physically based modelling by multiplicative cascade processes, in *Non-Linear Variability in Geophysics: Scaling and Fractals*, Schertzer, D. and Lovejoy, S., Eds., Kluwer, Boston, 185, 1991.

Yaglom, A. M., The influence on the fluctuation in energy dissipation of the shape of turbulent characteristics in the inertial interval, *Sov. Phys. Dokl.*, 2, 26, 1996.

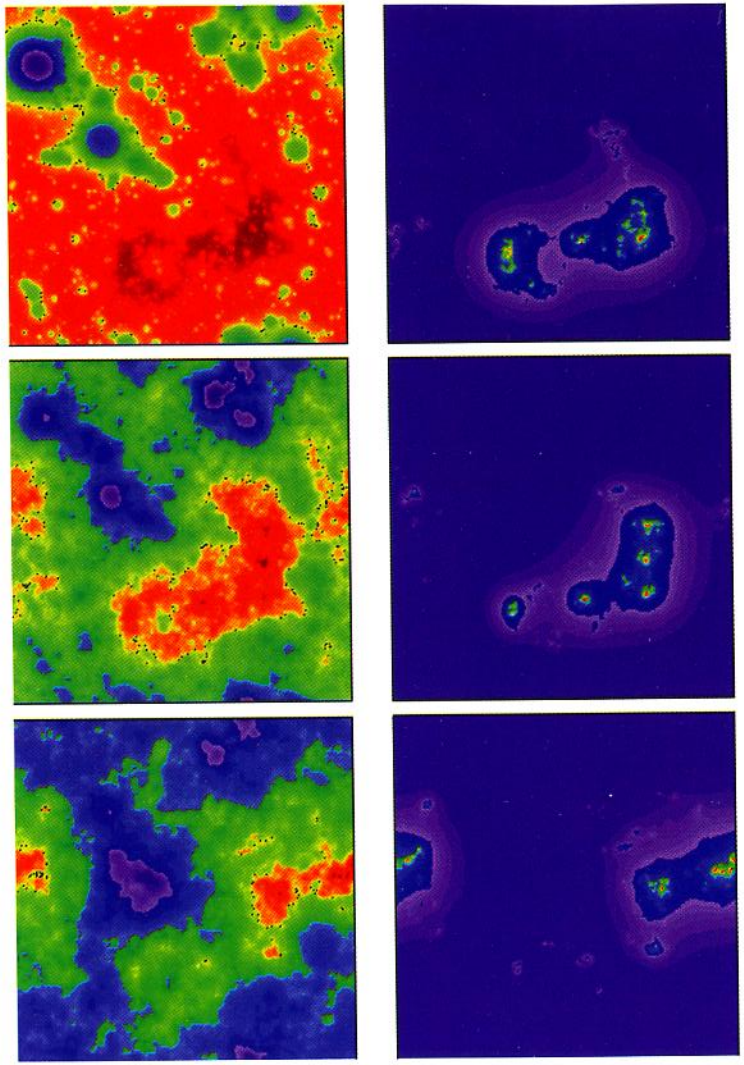

Plate 11 (Chapter 16) Simulated fields with varying multifractal parameters. The palette is rainbow, with high values red and low values purple. From top to bottom, $\alpha = 0.06$, 1.2, and 1.8. $C_1 = 0.05$ on the left and 1.2 on the right.

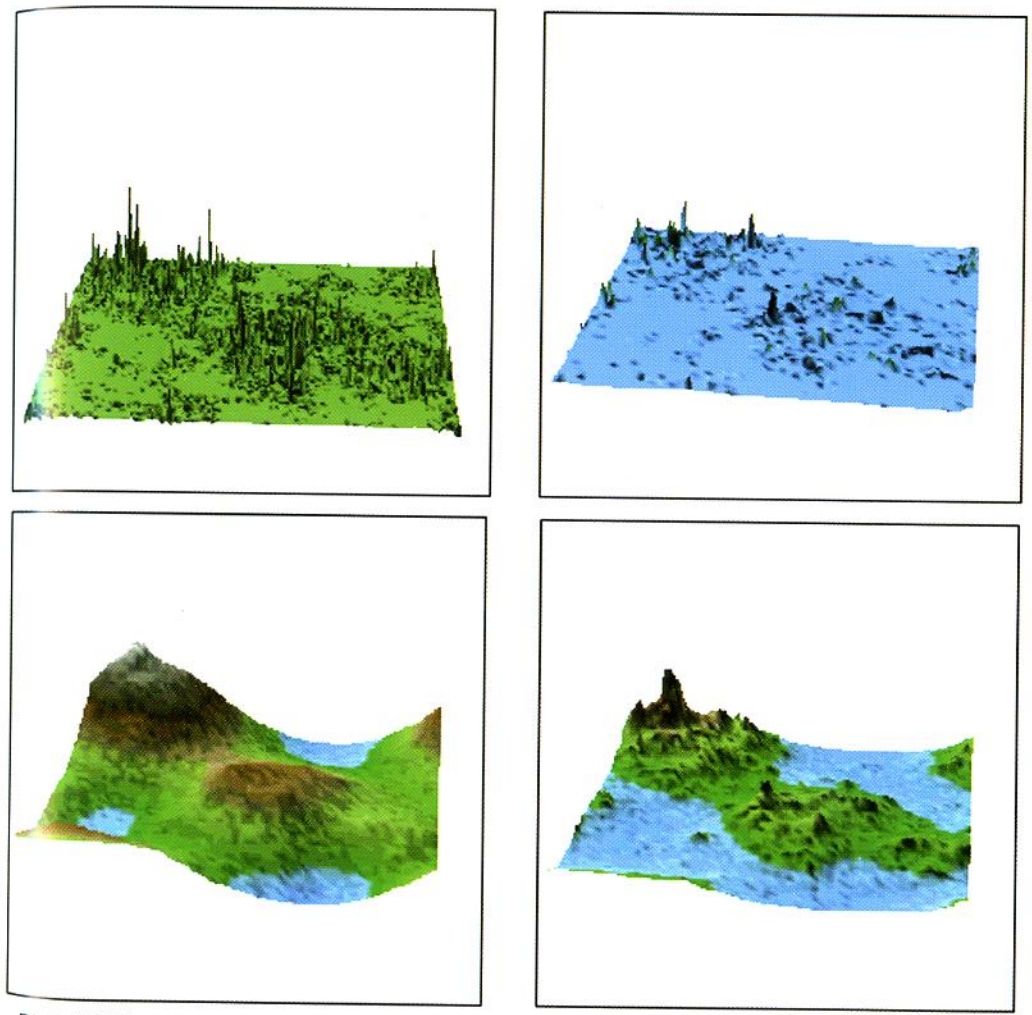

Plate 12 (Chapter 16) Varying the H-filter of the simulated field: $\alpha = 1.7$, $H = 0.05$. Clockwise from top left $H = -1.0$, $H = 0.0$, $H = 1.0$, $H = 2.0$

STEP 1: Generate a Lévy noise at each point, with the parameters α, a measure of the multifractality of the field, and C_1, the sparseness of the mean of the field.

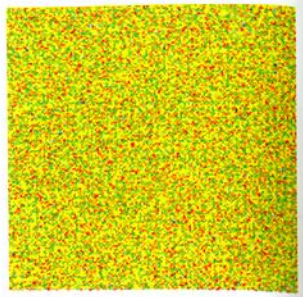

STEP 2: Fourier transform the noise.

STEP 3: Generate a filter $|\underline{k}|^{-d/\alpha'}$, with anisotropies given by the GSI parameters (using an anistropic norm); multiply the noise by this.

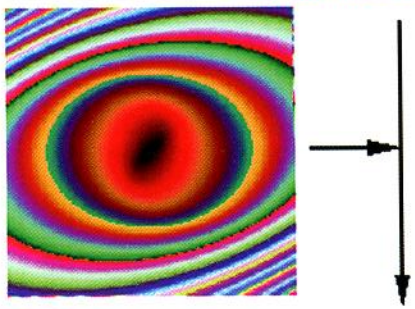

STEP 4: Inverse fourier transform the result. Steps 2 through 4 are the equivalent of a convolution of the noise with the appropriate filter.

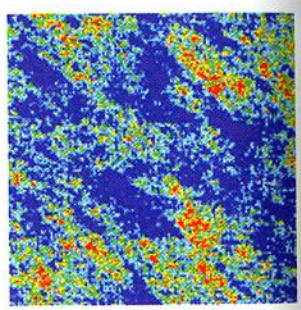

STEP 5: Exponentiate to obtain a real field.

STEP 6: Spectrally filter the field with a $|\underline{k}|^{-H}$ filter. This scale-invariant smoothing is in fact a fractional integration.

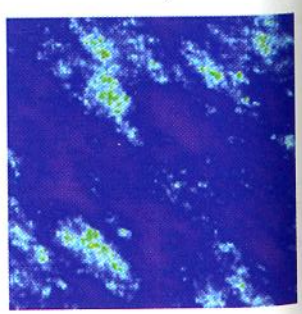

Plate 13 (Chapter 16) Simulating a universal multifractal field.

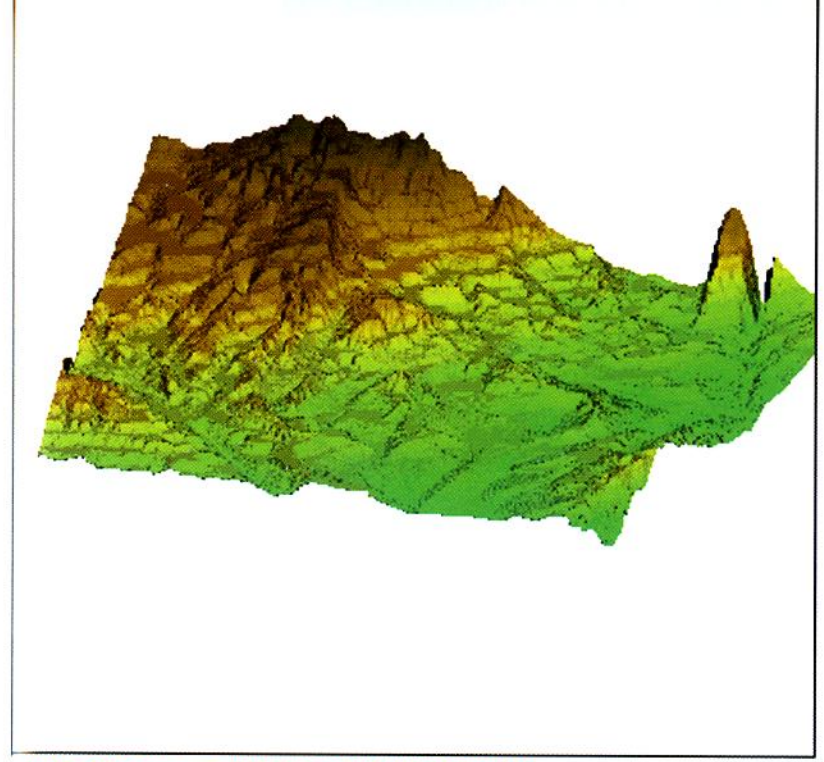

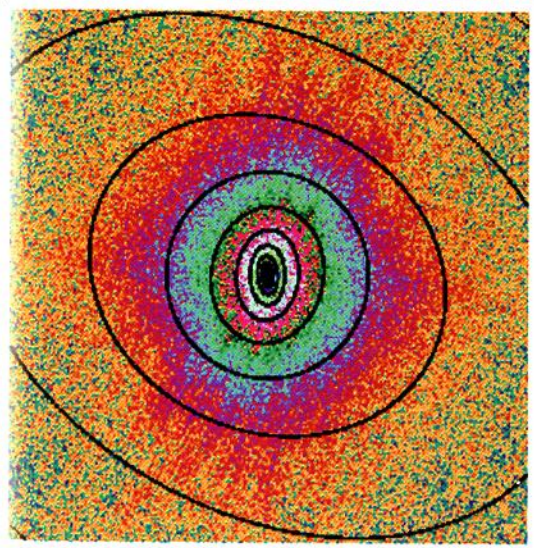

Plate 14 (Chapter 16)

Top. An example of U.S. landscape topography data, with 90-m resolution and size 512 x 512, visualized with ray-tracing. High values are brown; low values are green.

Bottom. The 2-D power spectrum of the data, showing anisotropies by the non-circular shapes. GSI parameters are $c = 0.15$, $f = -0.10$, and $e = 0.04$. The theoretical balls have been overlaid.

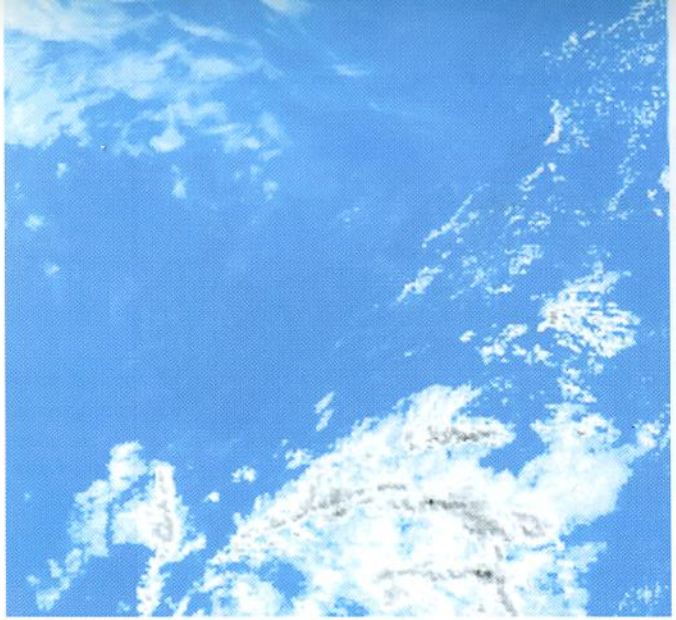

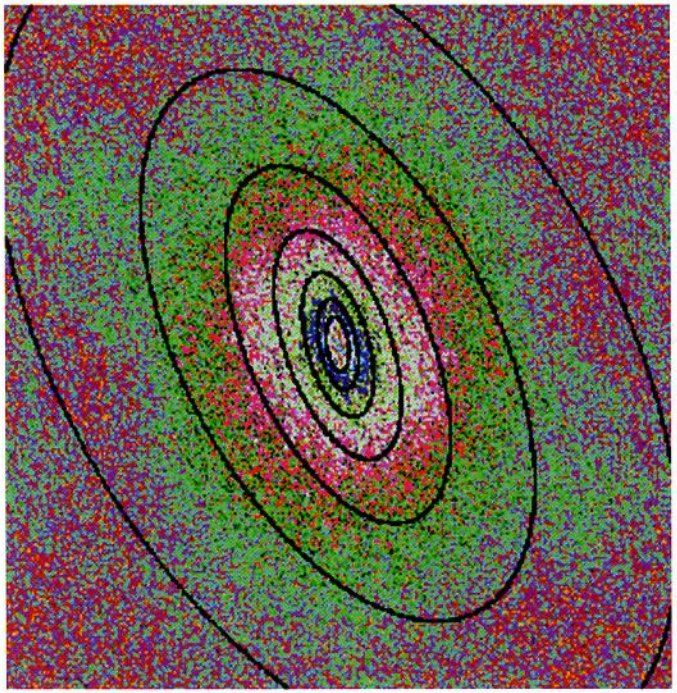

Plate 15 (Chapter 16)

Top. An example of AVHRR channel 1(visible spectrum) cloud data from NOAA-9 satellite, 1.1-km resolution, size 512x512.

Bottom. The 2-D power spectrum of the top image, showing stratification and differential rotation: the GSI parameters are $c = -0.04$, $f = 0.14$, and $e = 0.35$. Theoretical curves corresponding to this have been overlaid.

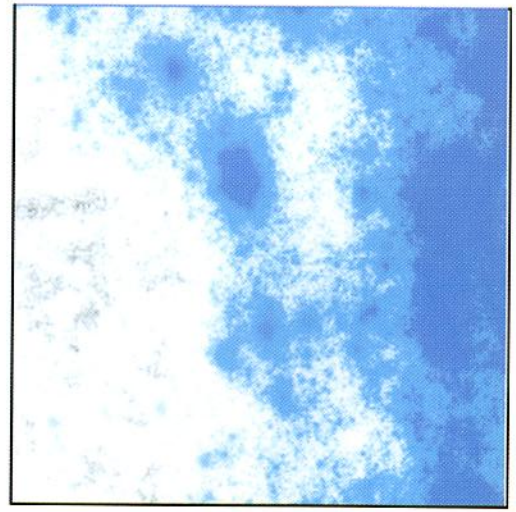

Plate 16 (Chapter 16)

Comparison of stratus cloud data (top) with simulated stratus (right top and bottom), using the measured parameters: $\alpha = 1.13$, $C_1 = 0.09$, $H = 0.4$, and GSI parameters of $c = 0.10$, $f = 0.0$, and $e = 0.05$, with a spheroscale of $\approx$ 5km.

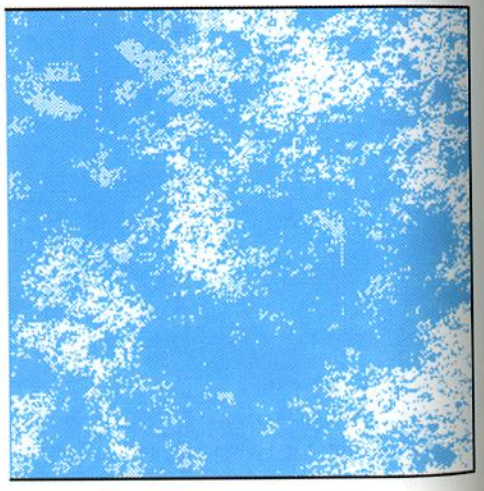

Plate 17 (Chapter 16)
Comparison of cumulus cloud data (top) with simulated cumulus (right top and bottom), using the measured parameters: $\alpha = 1.13$, $C_1 = 0.09$, $H = 0.4$ and GSI parameters of $c = 0.10$, $f = -0.5$, and $e = 0.30$, with a spheroscale of $\approx$ 30km.

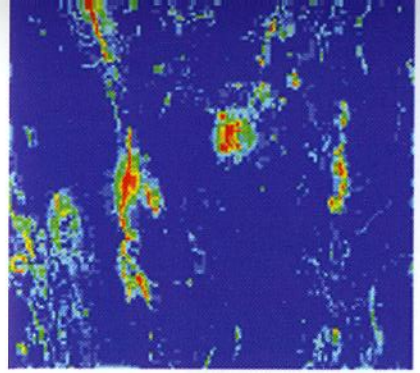

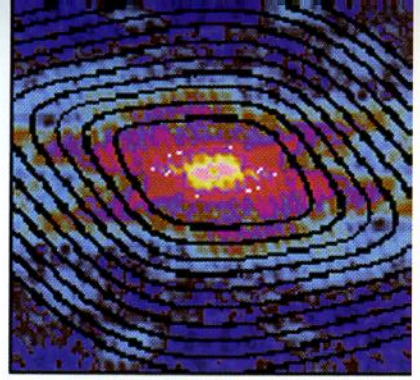

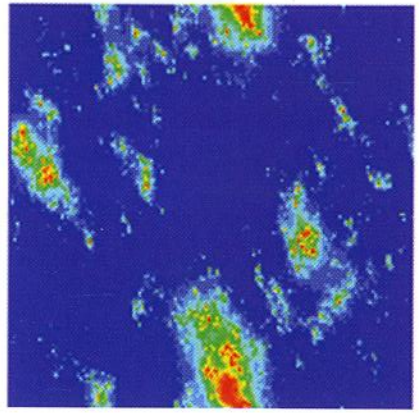

Plate 18 (Chapter 16)
Aeromagnetic anomaly data. Clockwise from top left, an aeromagnetic anomaly data set, its 2-D power spectrum, and a simulated field made using the measured parameters: $\alpha = 1.9$, $C_1 = 0.15$, and $H = 0.65$; and $c = 0.05$, $f = 0.10$, and $e = 0.22$. Note that for larger scales, the noise in the power spectrum of the data set alters the apparent shape of the balls.

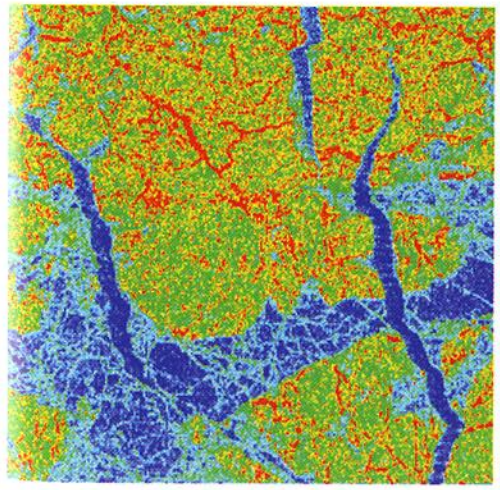

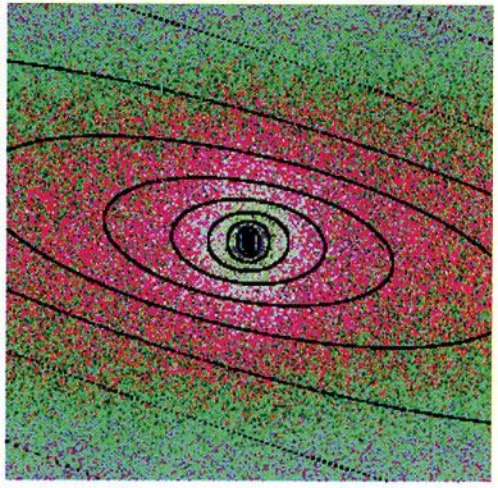

Plate 19 (Chapter 16) Sea ice radar reflectivity data. On the left is a data set, C band, polarization HH, with resolution of 12.5 m and size 512 x 512. On the right is its 2-D power spectrum. The GSI parameters measured were $c = 0.21$, $f = 0.0$, and $e = 0.0$.

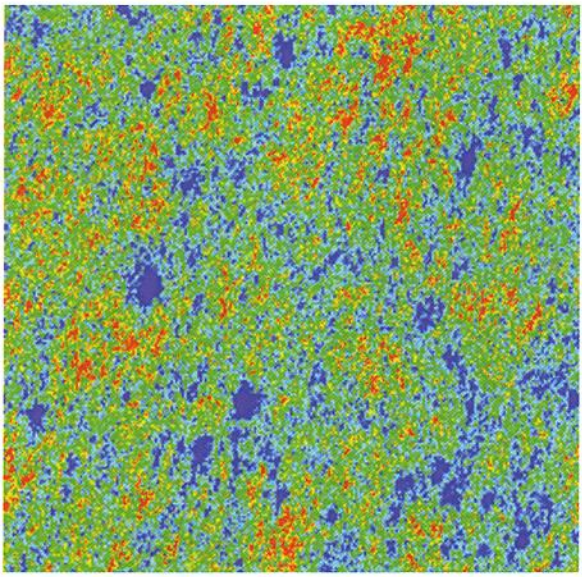

Plate 20 (Chapter 16) An example of simulated sea ice radar reflectivity, using $\alpha = 1.85$, $C_1 = 0.01$, $H = -0.10$. The GSI parameters used were $c = 0.21$, $f = 0.0$, and $e = 0.0$.

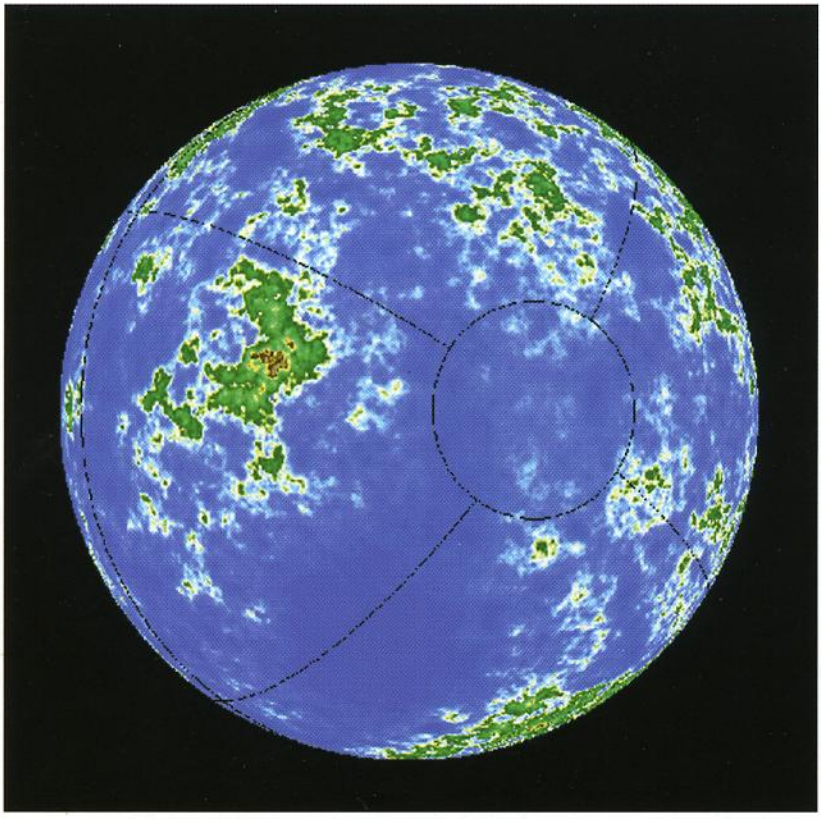

Plate 21 (Chapter 16) An example of simulated topography on a spherical surface (from Tan et al., 1996). Here, $\alpha = 1.7$, $C_1 = 0.10$, $H = 0.5$.